Big-bang nucleosynthesis and properties of stau

Programs in Science and Engineering

Course in Material Science

Toshifumi Jittoh

Abstract

In this thesis we investigate a problem of the big-bang nucleosynthesis in the minimal supersymmetric standard model. We find a solution to the problem and favored parameters of the supersymmetry.

Firstly we review the standard scenario of the big-bang nucleosynthesis. In the scenario there is a discrepancy of the abundance of ^{7}Li between the observation and the prediction of the big-bang nucleosynthesis. The discrepancy is called the lithium 7 problem. We find that a solution to the ^{7}Li problem can be given by a supersymmetric particle, stau.

Secondly we study the nature of the stau in a scenario in the minimal supersymmetric standard model. In our work the lightest supersymmetric particle (LSP) is a neutralino and the next lightest supersymmetric particle (NLSP) is a stau. The mass difference between the LSP and NLSP is expected as less than 1 % of neutralino mass since the abundance of dark matter is explained by this small mass difference. We evaluate the stau lifetime by calculating three decay modes; (1) the stau decay into the neutralino and tau, (2) the stau decay into the neutralino, tau-neutrino and pion, (3) the stau decay into the neutralino, tau-neutrino, electron(muon) and electron(muon)-neutrino, and discuss various parameters dependence of the stau lifetime. We find that the stau can survive until the big-bang nucleosynthesis era if the mass difference is less than 100 MeV.

At last we study a modification of the standard big-bang nucleosynthesis in this model to resolve the excessive theoretical prediction of the abundance of the primordial lithium 7 and beryllium 7. The stau provides a number of additional decay processes of lithium 7 and beryllium 7. A particularly important process is the internal conversion in the stau-nucleus bound state, which destroy the lithium 7 and beryllium 7 effectively. We calculate the internal conversion process with knowledge of nuclear physics. We show that the modification can lead to a prediction consistent with the observed abundance of lithium 7. Furthermore the solution to the lithium 7 problem gives favored properties of stau; the mass difference is (100 – 120) MeV and the yield value of stau is (7 – 10) $\times 10^{-10}$ by taking the mass of the neutralino as 300 GeV.

Contents

Chapter 1

Introduction

The theory of Big-Bang Nucleosynthesis (BBN) has been successful in predicting the abundance of light elements in the universe from a single parameter, baryon-to-photon ratio η. The recent results of the Wilkinson Microwave Anisotropy Probe (WMAP) experiment [1], however, put this theory into challenge. The extraordinarily precise results from WMAP are put together with the standard BBN (SBBN) to predict the abundance of ^{7}Li to be $(4.15^{+0.49}_{-0.45}) \times 10^{-10}$[2] if we adopt $\eta = 6.1 \times 10^{-10}$ (68 % C.L.) [1]. This prediction is inconsistent with the observation of metal-poor halo stars which implies $(1.23^{+0.32}_{-0.25}) \times 10^{-10}$ [3] reported by Ryan *et al.* [4]. The inconsistency persists even if we adopt the recent observations, which give the less restrictive constraint of $(2.19^{+0.30}_{-0.26}) \times 10^{-10}$ [5] and $(2.34^{+0.35}_{-0.30}) \times 10^{-10}$ [6]. This discrepancy can be hardly attributed to the correction of the cross section of nuclear reaction [7, 8], and astrophysical solutions are pursued [9].

Another interesting approach to this problem would be to consider effects induced by new physics beyond the Standard Model (SM). Exotic particles which interact with nuclei will open new channels to produce and destroy the nuclei, giving a potential solution to the ^{7}Li problem. In this paper we investigate a possibility that the interaction is initiated by a formation of bound state of an exotic negatively charged massive particles (CHAMPs) and a nucleus. (For the other solutions, see [10, 11, 12, 13, 14]).

So far the bound-state effects by CHAMPs have been attracting many interests [15, 16, 17, 18, 19, 20, 21, 22, 23]. For doubly-charged particles, see also Refs [24, 25, 26]. In particular, a significant enhancement of a ^{6}Li-production rate through $^4\text{He} + \text{D} \to {}^6\text{Li} + \gamma$ by the bound state with ^{4}He was reported [18] for the first time and recently confirmed [27]. This hinders the compatibility between particle physics models and BBN [28].

In addition, some nonstandard effects on the abundance of ^{7}Li and ^{7}Be were also considered in Ref. [19] and more recently in Ref. [29]. Introducing the CHAMPs with the mass of electroweak scale, the authors in Ref. [29] newly considered several destruction channels of ^{7}Be nuclei through the trapping of the CHAMPs to show that the abundance of the CHAMPs needs to be larger than 0.02 per baryon and that their lifetime has an allowed window between 1000 sec and 2000 sec.

We put the CHAMP BBN scenario in the minimal supersymmetric standard model (MSSM) with the conservation of R-parity. MSSM doubles the particle content of the SM by introducing the superparticles, which can accommodate the CHAMPs. The CHAMPs need lifetime long enough to sustain the sufficient abundance at the time of nucleosynthesis. Although the R-parity conservation stabilizes the lightest superparticles (LSPs), the observational constraints exclude charged superparticles as a candidate for LSPs, which is usually considered to be neutralinos $\tilde{\chi}^0$ or gravitinos. A possible candidate of CHAMPs is the next-lightest superparticle (NLSP) with electric charge, which can have long lifetime by assuming a small mass difference from the LSP [30].

We assume in the present paper that the LSP is a neutralino and the NLSP is a stau $\tilde{\tau}$, the superpartner of tau lepton τ. The staus can decay into neutralino LSP with the hadronic current, through which they also interact with the nuclei. The gravitino LSP, on the other hand, does not couple with hadronic current. We consider the bound state of ^{7}Be and $\tilde{\tau}^-$ in the early universe and the subsequent decay chain of nucleus $^7\mathrm{Be} \to {}^7\mathrm{Li} \to {}^7\mathrm{He}$ due to the interactions of the two. The ^{7}He nuclei rapidly decay into ^{6}He nuclei, which are effectively stable in the considered time scale. With the freedom of the mass of stau $m_{\tilde{\tau}}$ and its lifetime $\tau_{\tilde{\tau}}$, we search for the possible solution to the ^{7}Li problem that are phenomenologically acceptable.

This paper is organized as follows. In chapter 2 we overview the big bang nucleosynthesis and the ^{7}Li problem. We will find that some interactions which is caused by exotic particles are required to solve the problem. We will see the decay of stau in chapter 3 and find that staus have a possibility to solve the ^{7}Li problem. In chapter 4 we will see some interactions between stau and nuclei and find that stau-nucleus bound states play an important role in ^{7}Be/^{7}Li reducing processes. In chapter 5 we numerically calculate primordial abundances of light elements while taking into account the new channels. Then we will see the possible solution of ^{7}Li problem and favored properties of the stau. Finally, we summarize this thesis in chapter 6.

Chapter 2

Review of the Big-bang nucleosynthesis

In this chapter we review the big-bang nucleosynthesis (BBN). Here we see both of the theoretical and the experimental studies of the BBN. We will find a problem on the primordial abundance of the ^{7}Li, called ^{7}Li problem. At last we refer to that the Li problem can be solved in a beyond the standard model.

2.1 Thermal history of the universe

In this section we briefly overview the history of the universe. The history is depicted with thermal change. Our universe arose with a primitive fire ball so called "Big-bang". Immediately after the big-bang ($t = 10^{-43}$ sec), the temperature, T, of the universe was as high as the Planck scale ($T = 10^{19}$ GeV). After that the temperature decreases along with the expansion of the universe.

- $t \sim (10^{-37} - 10^{-33})$ sec or $T \sim (10^{16} - 10^{14})$ GeV
  A spontaneously symmetry breaking which breaks grand unified theory (GUT) occurred if GUT exist. The particles of the standard model (SM) appear in this time.

- $t \sim 10^{-10}$ sec or $T \sim 300$ GeV
  The electroweak symmetry is broken in this time, photons and electromagnetic interactions appear.

- $t \sim 10^{-4}$ sec or $T \sim 100$ MeV
  The chiral symmetry breaking occur. In this time color confinement occur, and protons and neutrons are formed.

- $t \sim (1 - 10^3)$ sec or $T \sim (1 - 0.01)$ MeV
  Light nuclei are synthesized in the universe. The abundances are precisely explained by the big-bang nucleosynthesis. The main theme of this thesis is a problem occurring in this time region.

- $t \sim 10^{12}$ sec or $T \sim 1$ eV
  The dominant component of the universe is changed from radiation to matter. In this time the formation of the structure begins.

- $t \sim 10^{13}$ sec or $T \sim 0.1$ eV
  In this era matter and radiation are decoupled since the small number density of the electron can not maintain the thermal equilibrium. The formation of atoms also occur in this era. Due to these phenomena photons be able to run straight, and the universe clear.

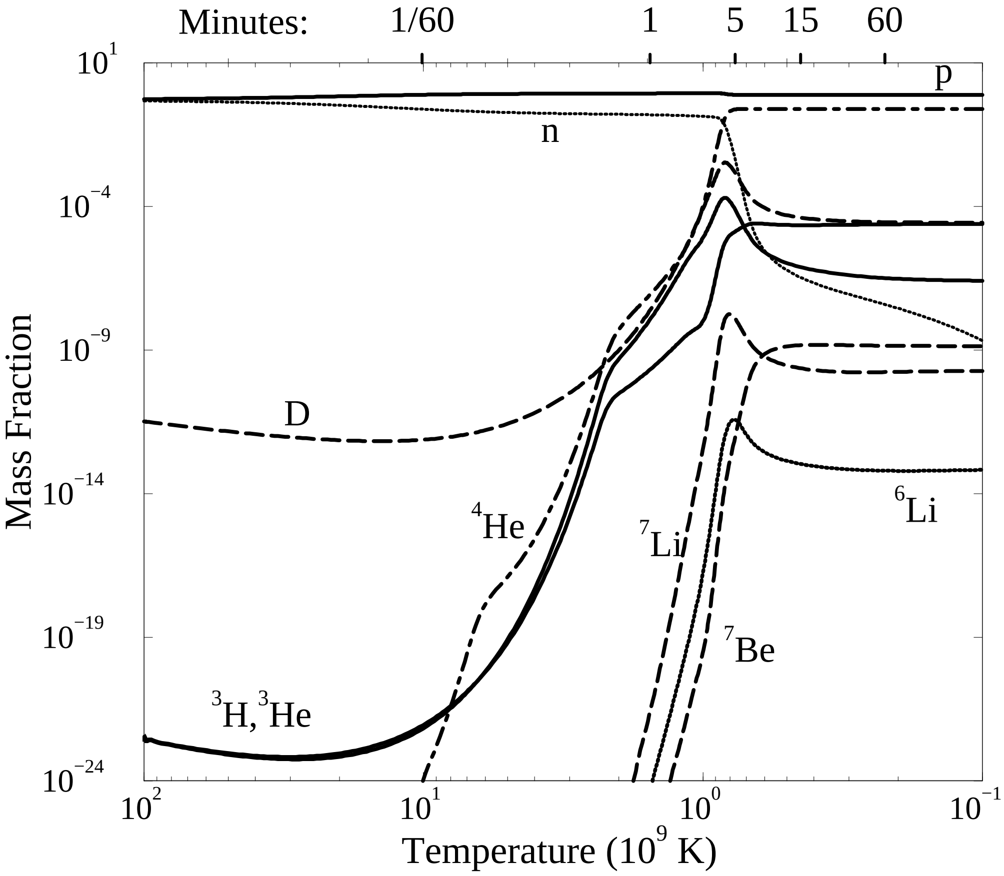

Figure 2.1: The time (thermal) evolution of the mass fractions of n, p, D, T+^{3}He, ^{4}He, ^{6}Li, ^{7}Li, ^{7}Be. Here the baryon-to-photon ratio $\eta = 5.1 \times 10^{-10}$. This figure is from Refs. [31].

2.2 Big-bang nucleosynthesis: Theory

In this and following two sections we concentrate to a time region, $t \sim (1 - 10^3)$ sec. Nuclei is firstly synthesized at this time region, and their abundances are well explained by the big-bang nucleosynthesis. In this section we see the BBN and its prediction. We will see observed value of the abundances in the next section.

The results of the big-bang nucleosynthesis is shown in Figs. 2.1 which is from Refs. [31]. The figure shows the time and thermal evolution of the mass fractions of n, p, D, T+^{3}He, ^{4}He, ^{6}Li, ^{7}Li, ^{7}Be. The range of the figure, 10^{11} K – 10^8 K, corresponds to 10 MeV – 10 keV. The nucleosynthesis is understood via three steps along with the change of the temperature of the universe; (1) $T \simeq 10$MeV, (2) $T \simeq 1$MeV, (3) $T \simeq 0.1$MeV. In this figure the baryon-to-photon ratio η is taken as 5.1×10^{-10}.

2.2.1 Synthesis processes

1. **$T \simeq 10$MeV; Nuclear statistical equilibrium**
   The number densities of nuclei is determined by nuclear statistical equilibrium, when the temperature of the universe is about 10 MeV. In nuclear statistical equilibrium forming and deforming

nuclear species	binding energy
deuteron	2.22 MeV
tritium	6.92 MeV
helium 3	7.72 MeV
helium 4	28.3 MeV
carbon 12	46.1 MeV

Table 2.1: The mass fraction for the proton, neutron, deuteron, helium 3, helium 4 and carbon 6 in the nuclear statistical equilibrium.

processes of nuclei,

$$Z \cdot p + (A - Z) \cdot n \leftrightarrow A(Z), \tag{2.1}$$

are overcoming the expansion rate of the universe. The number density of a nucleus, $A(Z)$, which has mass number A and proton number Z is determined by the number densities of proton and neutron, n_p and n_n, and the binding energy of the nucleus, B_A;

$$n_A = g_A A^{3/2} 2^{-A} \left(\frac{2\pi}{m_N T} \right)^{\frac{3(A-1)}{2}} n_p^Z n_n^{A-Z} \exp\left(\frac{B_A}{T} \right), \tag{2.2}$$

where g_A is the axial vector coupling constant, m_N is the nucleon mass and T is the temperature of the universe. The binding energies of each nucleus are listed in Table 2.1. Here carbon 12 is chose as an example of “metal”.

The number density is not invariant and is reduced by expansion of the universe. Therefore a useful representation of the number of a nucleus is mass fraction;

$$X_A \equiv \frac{n_A A}{n_N}, \tag{2.3}$$

where n_N is total nucleon density defined as,

$$n_N = n_n + n_p + \sum A \cdot n_A. \tag{2.4}$$

Here the summation runs all nuclear species.

The mass fraction of a number density of a nucleus, $A(Z)$ is

$$X_A = g_A \left[\zeta(3)^{A-1} \pi^{\frac{1-A}{2}} 2^{\frac{3A-5}{2}} \right] A^{\frac{5}{2}} \left(\frac{T}{m_N} \right)^{\frac{3(A-1)}{2}} \eta^{A-1} X_p^Z X_n^{A-Z} \exp\left(\frac{B_A}{T} \right), \tag{2.5}$$

where $\zeta(x)$ is zeta function and X_p and X_n are mass fraction of proton and neutron, respectively. $\eta \sim 10^{-10}$ is the baryon-to-photon ratio. The most precise value of η is given by the WMAP experiment [1],

$$\eta = (6.225 \pm 0.170) \times 10^{-10}. \tag{2.6}$$

The value of the mass fraction for the proton, neutron, deuteron, D, helium 3, ^{3}He, helium 4, ^{4}He and carbon 12, ^{1}2C, at $T = 10$ MeV are listed in Table 2.2. Nuclei is not formed at this temperature since the smallness of the η, and almost nucleons are still free. The ratio of the mass fractions of

nuclear species	mass fraction
proton	$\simeq 0.5$
neutron	$\simeq 0.5$
deuteron	$\simeq 6 \times 10^{-12}$
helium 3	$\simeq 2 \times 10^{-23}$
helium 4	$\simeq 2 \times 10^{-34}$
carbon 12	$\simeq 2 \times 10^{-126}$

Table 2.2: The mass fraction for the proton, neutron, deuteron, helium 3, helium 4 and carbon 12 in the nuclear statistical equilibrium.

proton and neutron is one since mass difference between proton and neutron is negligible when the temperature of the universe is about 10 MeV. Thus the nucleosynthesis occur at the lower temperature.

2. **$T \simeq 1$MeV; freeze out of neutron to proton ratio**
   In this time region the weak interaction interconverting proton and neutron;

$$n + e^+ \leftrightarrow p + \bar{\nu_e}, \tag{2.7}$$
$$n + \nu_e \leftrightarrow p + e^-, \tag{2.8}$$
$$n \leftrightarrow p + e^- + \bar{\nu_e}, \tag{2.9}$$

   freeze out. The neutron to proton ratio at the freeze out time is same with the value in the nuclear statistical equilibrium,

$$\left(\frac{n}{p}\right)_{\text{freeze out}} = \exp\left(-\frac{Q}{T_F}\right) \simeq \frac{1}{6}, \tag{2.10}$$

   where Q is the mass difference between proton and neutron, and T_F is the temperature of the universe at the freeze out time.

   From the freeze out till beginning of nucleosynthesis the neutron to proton ratio is changed by the spontaneous decay of the neutrons. The value at the beginning of the nucleosynthesis becomes 1/7. The change of the neutron to proton ratio is significant to estimate the primordial abundances of the nuclei.

3. **$T \simeq 0.1$MeV; nucleosynthesis**
   According with the decreasing temperature nucleosynthesis begins. At $T \simeq 0.1$MeV the nuclear statistical equilibrium is not maintained since nuclear formation rate loose the expansion rate of the universe. Therefore the mass fractions of nuclei deviate from the values of nuclear statistical equilibrium, and the nucleosynthesis begins. We see synthesis processes of each nuclei; D, ^{4}He, ^{3}He, T, ^{7}Li and ^{6}Li.

   (a) **Deuteron**
   Deuteron is synthesized before anything else. Other elements are synthesize by using the deuteron as fuel.

   A dominant producing process of deuterons is

$$n + p \to \mathrm{D} + \gamma. \tag{2.11}$$

We note that only 2-body reactions are important for not only producing process of deuteron but also that of other nuclei since the density has become rather low by this time. A reducing process of deuterons is induced by background photons,

$$\mathrm{D} + \gamma \to n + p, \tag{2.12}$$

The producing process overcomes the reducing process when the number density of the deuteron n_{D}, becomes larger than the number density of photons with the energy larger than the binding energy of deuteron, 2.22 MeV, $n_{\gamma\text{-}2.22\mathrm{MeV}}$. The number densities are roughly estimated as,

$$n_{\gamma\text{-}2.22\mathrm{MeV}} = n_\gamma \exp\left(-\frac{2.22\ \mathrm{MeV}}{T}\right), \tag{2.13}$$

$$n_{\mathrm{D}} = \eta \cdot n_\gamma \tag{2.14}$$

where n_γ is the number density of photon, T is the temperature of the universe and η is the baryon-to-photon ratio which is $\mathcal{O}(10^{-10})$. Therefore when $T \lesssim 0.1$ MeV, the producing process overcomes the reducing process and syntheses of other nuclei occur.

(b) **Helium 4**

After the synthesis of deuterons, helium 4 is synthesized via the following processes,

$$\mathrm{D} + p \to {}^3\mathrm{He} + \gamma, \tag{2.15}$$
$$\mathrm{D} + n \to \mathrm{T} + \gamma, \tag{2.16}$$
$$\mathrm{D} + \mathrm{D} \to {}^4\mathrm{He} + \gamma, \tag{2.17}$$
$$\mathrm{T} + p \to {}^4\mathrm{He} + \gamma, \tag{2.18}$$
$${}^3\mathrm{He} + n \to {}^4\mathrm{He} + \gamma, \tag{2.19}$$
$$\mathrm{D} + \mathrm{D} \to {}^3\mathrm{He} + n, \tag{2.20}$$
$$\mathrm{D} + \mathrm{D} \to \mathrm{T} + p, \tag{2.21}$$
$${}^3\mathrm{He} + n \to \mathrm{T} + p, \tag{2.22}$$
$$\mathrm{T} + \mathrm{D} \to {}^4\mathrm{He} + n, \tag{2.23}$$
$${}^3\mathrm{He} + \mathrm{D} \to {}^4\mathrm{He} + p. \tag{2.24}$$

Here the processes (2.15)–(2.19) are induced by the strong and the electromagnetic interactions, while the processes (2.20)–(2.24) are induced by only the strong interaction. Almost of neutrons are taken in in ^{4}He via above processes since ^{4}He is most stable nucleus. Therefore the abundance of ^{4}He is roughly determined by the neutron to proton ratio,

$$Y \equiv X_{^4\mathrm{He}} = \frac{2(n_n/n_p)}{1 + (n_n/n_p)} \simeq 0.25, \tag{2.25}$$

where we use $n_n/n_p = 1/7$ which is the neutron to proton ratio at the beginning time of nucleosynthesis.

(c) **Helium 3 and Triton**

Helium 3 and Triton are also synthesized via processes (2.15), (2.16) and (2.20)–(2.22). They, however, become ^{4}He via the processes (2.18), (2.19), (2.22) and (2.23) since ^{4}He is more stable than ^{3}He and T. Therefore the abundances of ^{3}He and T is much lower than of ^{4}He.

Triton is unstable and decay into Helium 3 with half-life 12.32 years. Therefore ^{3}He abundance observed today is total synthesized value of ^{3}He and T.

(d) **Lithium 6, 7 and Beryllium 7**

We next consider the synthesis of ^{6}Li, ^{7}Li and ^{7}Be. The syntheses of nuclei heavier than ^{4}He encounter two obstacles. First obstacle is absence of stable nucleus with mass number five and eight. The structure of nuclei with mass number five is described as (i) a core of ^{4}He and orbital nucleon, or (ii) a deuteron and three neutrons or protons, or (iii) five neutrons or protons. In the case (i) interactions between nucleons in ^{4}He are much stronger than between ^{4}He and orbital nucleon. Therefore the orbital nucleon easily separate from ^{4}He core. In the case (ii) the deuteron and neutrons are also weakly interacted and easily separate each other, and in the case (iii) the interactions between five neutrons or protons are weak, and they separate easily. The structure of nuclei with mass number eight is described as (i) two cores of ^{4}He, or (ii) one ^{4}He, one deuteron and two neutrons or protons, or (iii) one ^{4}He and four neutrons or protons, or (iv) one deuteron and six neutrons or protons, or (v) eight neutrons or protons. In the case (i) the cores are weakly bound, and thus easily separate from each other. Apparently the cases (ii)–(v) are less stable than case (i) and thus they are not stable.

The second obstacle is the Coulomb barrier. At the formation time of heavy nuclei the effect of the Coulomb barrier is not negligible, since the momentum energy of heavier nuclei at its formation time is smaller than that of lighter nuclei. Furthermore heavier nuclei have larger electric charge and are affected stronger force by the Coulomb barrier. Due to the obstacles lithium and beryllium are synthesized only slightly, and synthesis of the nuclei heavier than beryllium is practically impossible.

Production processes of ^{6}Li, ^{7}Li and ^{7}Be are as follows,

$$^4\mathrm{He} + \mathrm{D} \to {}^6\mathrm{Li} + \gamma, \tag{2.26}$$

$$^3\mathrm{He} + \mathrm{T} \to {}^6\mathrm{Li} + \gamma, \tag{2.27}$$

$$^4\mathrm{He} + \mathrm{T} \to {}^7\mathrm{Li} + \gamma, \tag{2.28}$$

$$^4\mathrm{He} + {}^3\mathrm{He} \to {}^7\mathrm{Be} + \gamma. \tag{2.29}$$

The ^{7}Be is unstable and becomes ^{7}Li due to the electron capture with the half-life 53.22 days,

$$^7\mathrm{Be} \xrightarrow[\text{53.22 days}]{\text{electron capture}} {}^7\mathrm{Li}. \tag{2.30}$$

The decay of ^{7}Be occurs after BBN era. Therefore ^{7}Li abundance observed today is total synthesized value of ^{7}Li and ^{7}Be.

2.2.2 Parameter dependence

Theoretical values of the abundances of the nuclei are depend on some parameters.

baryon-to-photon ratio η

As we can see from Eq. (2.5), mass fractions of nuclei depend on the baryon-to-photon ratio η. If η is large (i.e. the baryon number density is large), the synthesis of nuclei begins earlier. Therefore larger value of deuteron and helium 3 which behave as fuel are burned, and thus their abundances become smaller. According to earlier syntheses of D and T, synthesis of helium 4 also begins earlier. However the abundance of ^{4}He changes slightly since the abundance is determined by the neutron to proton ratio.

The η dependence of the ^{7}Li abundance is not monotonic. Along with the increase of η, the ^{7}Li abundance decreases monotonically for $\eta \lesssim 3 \times 10^{-9}$, while it increase monotonically for $\eta \gtrsim 3 \times 10^{-9}$.

This is due to a replacement of dominant ^{7}Li (^{7}Be) synthesis processes. The dominant process for $\eta \lesssim 3 \times 10^{-9}$ is (2.28), while for $\eta \gtrsim 3 \times 10^{-9}$ is (2.29).

Figure 2.2 which is from Ref. [32] shows the η dependence of the abundances of ^{4}He, D, ^{3}He+T and ^{7}Li. The width of the bands shows the 95% cl range. Boxes indicate the observed light element abundances (smaller boxes: $\pm 2\sigma$ statistical errors; larger boxes: $\pm 2\sigma$ statistical and systematic errors). The narrow vertical band indicates the CMB measure of the baryon density, while the wider band indicates the BBN concordance range (both at 95% cl).

The abundances of ^{4}He, D, ^{3}He and ^{7}Li at the observed η are given by Ref. [2];

$$Y_p = 0.2479 \pm 0.0004, \tag{2.31}$$

$$\mathrm{D/H} = 2.60^{+0.19}_{-0.17} \times 10^{-5}, \tag{2.32}$$

$$^3\mathrm{He/H} = (1.04 \pm 0.04) \times 10^{-5}, \tag{2.33}$$

$$^7\mathrm{Li/H} = 4.15^{+0.49}_{-0.45} \times 10^{-10}. \tag{2.34}$$

relativistic degree of freedom g_*

The relativistic degree of freedom g_* affect to the freeze out time of nuclear statistical equilibrium and beginning time of nucleosynthesis since the expansion rate of the universe depends on g_*. The relativistic degree of freedom is a function of the temperature of the universe and determined by the number and spin of relativistic particles,

$$g_* \equiv \sum_{i=\mathrm{bosons}} g_i \left(\frac{T_i}{T}\right)^4 + \frac{7}{8} \sum_{i=\mathrm{fermions}} g_i \left(\frac{T_i}{T}\right)^4. \tag{2.35}$$

Relativistic particles at the BBN era are photon and neutrinos of three generations in the standard model of elementary particle physics. If there exist other relativistic particles, g_* will be larger.

Larger g_* leads larger expansion rate of the universe since the rate is proportional to $\sqrt{g_*}$, and therefore earlier breaking of nuclear statistical equilibrium and nucleosynthesis. This fact can be used to constraint of generation number of neutrino. In this thesis we consider only standard model particles and its superpartners, and thus three generation of neutrino.

neutron lifetime τ_n

The weak interaction rates of the processes (2.7) – (2.9) are proportional to inverse neutron lifetime τ_n^{-1}. Therefore larger τ_n leads smaller weak interaction rate, and earlier freeze out of neutron to proton ratio, and thus larger mass fraction of ^{4}He. The lifetime is recently well investigated by experiments and its uncertainty has been reduced.

2.2.3 Calculation of the big-bang nucleosynthesis

The prediction of the BBN for the light element abundances is given by numerical simulation. By calculating a nuclear reactions network such as shown in Fig. 2.3 we simulate the nucleosynthesis process occurred in the early universe.

The simulation of the nucleosynthesis have been developed continuously. A calculation code for the ^{4}He abundance was written by Alpher, Follin and Herman [34] in 1953. In 1966 Peebles wrote a very simple code to follow ^{4}He synthesis [35]. In 1967 Wagoner, Fowler and Hoyle wrote a very detailed reaction network to follow primordial nucleosynthesis [36]. A code was written by Wagoner in 1973 [37] and becomes “standard code” for primordial nucleosynthesis. The code has been updated by correcting nuclear reaction rates, the effect of finite temperature, procedure of calculation and so on. Now so called

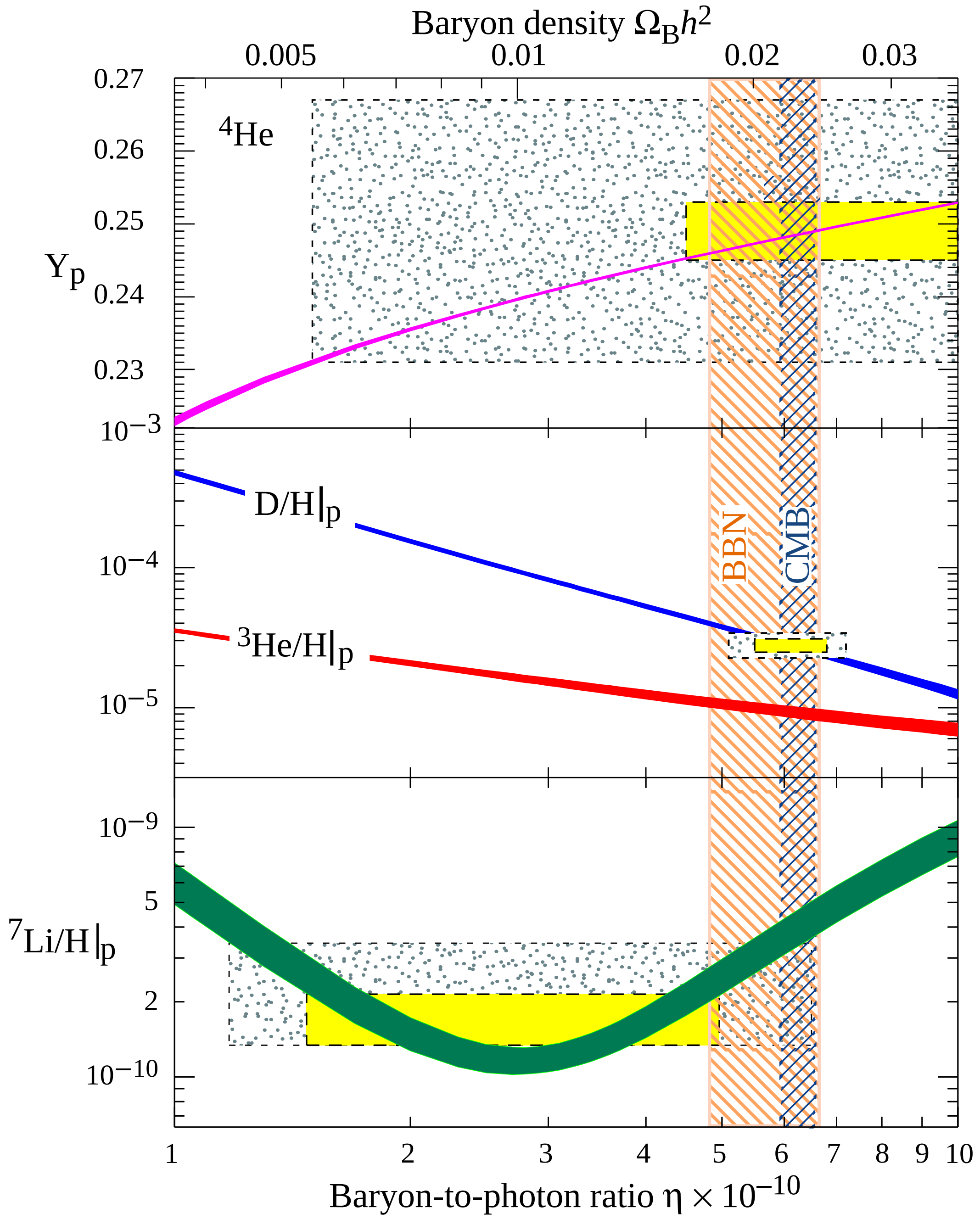

Figure 2.2: The η dependence of the abundances of ^{4}He, D, ^{3}He+T and ^{7}Li. The width of the bands shows the 95% cl range. Boxes indicate the observed light element abundances (smaller boxes: $\pm 2\sigma$ statistical errors; larger boxes: $\pm 2\sigma$ statistical and systematic errors). The narrow vertical band indicates the CMB measure of the baryon density, while the wider band indicates the BBN concordance range (both at 95% cl). This figure is from Ref. [32].

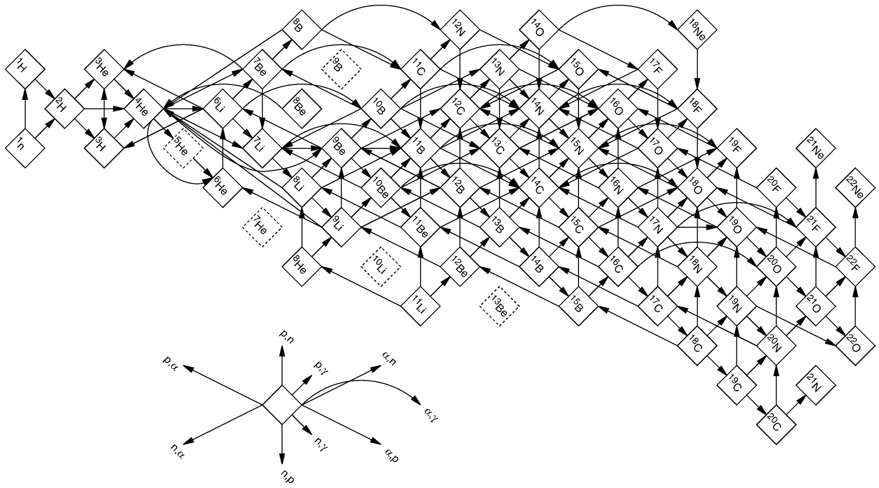

Figure 2.3: Nuclear reactions network. This figure is from Ref. [33].

"Kawano code" [38] and its updated version is used commonly. We use one of the updated code in this thesis.

2.3 Big-bang nucleosynthesis: Observation

In this section we investigate observations of the primordial abundances. Before going to see the discussion of observations for each elements we consider the general condition for the observed objects. The important point for the observation of primordial abundance is whether the value is truly "primordial". Nuclear fusion in stars, supernovae and photonuclear reaction processes change the primordial mass fractions. Therefore we must observe the value without above changing processes. A good criterion to judge whether a value is primordial or not is metallicity. In a object with low metallicity we can find the primordial value since metals are created in not the early universe but star and supernovae. We parametrize the metallicity by logarithm of mass fraction of Fe normalized by solar metallicity,

$$[\mathrm{Fe/H}] \equiv \log_{10}\left(\frac{N_{\mathrm{Fe}}}{N_{\mathrm{H}}}\right)_{object} - \log_{10}\left(\frac{N_{\mathrm{Fe}}}{N_{\mathrm{H}}}\right)_{sun}. \tag{2.36}$$

Here N_{Fe} and N_{H} are number densities of Fe and p, respectively. Subscripts, *objects* and *sun*, means the value of observed object and sun, respectively.

2.3.1 ^{4}He

We observe ^{4}He in recombination line from extragalactic HII regions *. In HII regions there are not only H^+ but also He^+. They recombine and ionize as follows;

$$\mathrm{H}^+ + e^- \leftrightarrow \mathrm{H} + \gamma \tag{2.37}$$

$$\mathrm{He}^+ + e^- \leftrightarrow \mathrm{He} + \gamma \tag{2.38}$$

*HII means a ionized atom H^+. The Roman number shows the level of ionization; e.g. II means 1+, III means 2+, IV means 3+, $\cdots$. For example, HeIII means He^{2+}.

The emitted γ which is called recombination line in the above processes have specific wavelength. The wavelengths of recombination line of these ions are different.

We can evaluate the ratio of the primordial abundances of helium 4 and hydrogen [^{4}He/H] by comparing the strength of the recombination lines of H^+ and He^+ since almost hydrogen and helium 4 is in H^+ and He^+, respectively. Typical temperature of HII region is 1 eV and smaller than the ionization energy of He^+, 24.6 eV, then the number of photons with 24.6 eV is strongly suppressed by the Boltzmann factor $e^{-E/T} \sim 10^{-11}$. However the total number of photons is larger than the number of ^{4}He which is quarter of the baryon number since baryon-to-photon ratio η is about 10^{-10}. Therefore the number of photons with 24.6 eV $n_\gamma|_{24.6\mathrm{eV}}$ is same order of the number of helium 4;

$$n_\gamma|_{24.6\mathrm{eV}} \sim n_\gamma e^{-E/T} \sim \frac{4n_{^4\mathrm{He}}}{\eta} 10^{-11} \sim n_{^4\mathrm{He}}. \tag{2.39}$$

Due to the same consideration we can see that He^{2+} is not in HII region since the number of photons with the ionization energy of He^{2+}, 54.4 eV, is suppressed by the Boltzmann factor 10^{-24}.

Helium 4 is created by nuclear fusion process in stars, and thus the observed helium to hydrogen ratio may not be primordial one. To identify the ratio is primordial, we use the metallicity as a measure. In stars helium 4 and metals are created together, and created values of them are positively correlated. Therefore by observing metal poor HII region, determining the correlation and extrapolating to zero-metallicity, we find primordial helium to hydrogen ratio. The most metal poor HII regions are in distant blue compact galaxies. The observed primordial ^{4}He abundance given by Ref. [39] is

$$Y_\mathrm{p} = 0.249 \pm 0.009. \tag{2.40}$$

Even though the error includes both of statistical and systematic one, it is dominated by systematic one since it is depends on physical property of HII region and thus has large uncertainty. This value is shown in Fig. 2.2.

There are some other observed value of Y_P; e.g. $Y_\mathrm{p} = 0.2472 \pm 0.0012$ and $Y_\mathrm{p} = 0.2516 \pm 0.0011$ depending on which set of HeI emissivities are used [40]. These values are,however, consistent within the margin of error.

2.3.2 D

Deuteron is most precisely observed in high-redshift, low metallicity quasar absorption system, via its isotope-shifted Lyman-α absorption. Elements in gas absorb the light with specific energies (wavelengths) from quasars. We can find the existence of elements in the gas by the absorption. Deuterons absorb the isotope-shifted Lyman lines whose energy is determined by subtracting the energy of electron in ground state from in n-th orbital state;

$$\frac{m_e m_\mathrm{D} e^4}{2(m_e + m_\mathrm{D})}\left(1 - \frac{1}{n^2}\right), \tag{2.41}$$

where m_D is the mass of deuteron. A absorption line with $n = 2, 3, 4, \cdots$ is called the Lyman-α, -β, -γ, $\cdots$, respectively. The Lyman lines of hydrogen are obtained by substituting m_D with m_p. The energy of the Lyman-α line of deuteron is 0.025% larger than that of hydrogen. By comparing the strength of the Lyman-α lines of deuteron and hydrogen, we can evaluate the primordial value of the deuteron to hydrogen ratio;

$$[\mathrm{D/H}]_\mathrm{p} = (2.84 \pm 0.14) \times 10^{-5} \quad \text{(with only statistical error)}, \tag{2.42}$$

$$[\mathrm{D/H}]_\mathrm{p} = (2.84 \pm 0.26) \times 10^{-5} \quad \text{(with statistical and systematic errors)}, \tag{2.43}$$

where subscript p means primordial value. These values are given in Ref. [32]. The value (2.42) corresponds to smaller box in Fig. 2.2, while the value (2.43) corresponds to larger box in Fig. 2.2.

Smaller values of the abundance is reported by some works; e.g. in Ref. [41] $[\mathrm{D/H}]_\mathrm{p} = (1.56 \pm 0.04) \times 10^{-5}$ is reported by a observation for interstellar medium within ∼100 pc of the Sun. However we adopt the values in (2.42) and (2.43) since there is no astrophysical process producing deuterons in the universe after the BBN, and thus observed value gives a lower limit to primordial D/H.

2.3.3 ^{3}He

The primordial value of $[^3\mathrm{He/H}]$ has been measured only in galactic HII regions [42]. In the reference [42] the primordial ^{3}He value is evaluated as,

$$[^3\mathrm{He/H}]_\mathrm{p} = (1.1 \pm 0.2) \times 10^{-5} \tag{2.44}$$

This value is, however, unreliable since this is not directly observed one.

We can obtain the upper limit of the primordial ^{3}He abundance by considering a ratio $[^3\mathrm{He/D}]$. The ratio increases monotonically with progress of nuclear reactions in astronomical objects. Therefore the observed value of $[^3\mathrm{He/D}]$ is larger than primordial value and becomes upper limit. The value is given in Ref.[43],

$$[^3\mathrm{He/D}]_\mathrm{p} < 0.83 + 0.27. \tag{2.45}$$

2.3.4 ^{7}Li

The ^{7}Li abundance is observed in absorption line from metal poor Pop II stars in our galaxy. Here Pop II star is the oldest stars in observed ones and parent generational stars of sun. Its metallicity is going down to at least 10^{-4} and perhaps 10^{-5}. The ^{7}Li abundance does not vary significantly with metallicity and temperature in Pop II stars. This feature is called "Spite plateau" [44]. In Fig. 2.4 which is from Ref. [6], the *plateau* is shown. The upper panel shows $\mathrm{A_{Li}}$ of the Spite plateau stars ($T_\mathrm{eff} > 6000$K) as a function of [Fe/H]. Here $\mathrm{A_{Li}}$ is defined as,

$$\mathrm{A_{Li}} \equiv \log([^7\mathrm{Li/H}]) + 12. \tag{2.46}$$

The dotted line indicates the mean ^7Li abundance of the plateau stars, and the solid line represents the lower limit imposed by the WMAP constraint. The error bars indicate the predicted error, σ_pred ($= 10^{0.05} \simeq 1.12$), and $3\sigma_\mathrm{pred}$ ($= 10^{0.15} \simeq 1.41$). The lower panel shows $\mathrm{A_{Li}}$ as a function of T_eff for stars with $[\mathrm{Fe/H}] \leq -1.5$ (filled triangles) and $[\mathrm{Fe/H}] > -1.5$ (open triangles). The star (HD106038) with the highest Li abundance (open triangle inside the open circle) is a star with peculiar abundances [45].

Recent precise measurements find that the abundance slightly correlates with metallicity. The correlation can be understood as the result of ^{7}Li production from galactic cosmic ray [46]. By extrapolating to zero metallicity, we obtain a primordial value [3],

$$[^7\mathrm{Li/H}]_\mathrm{p} = (1.23 \pm 0.06) \times 10^{-10}. \tag{2.47}$$

There are many different observed values; e.g.

$$[^7\mathrm{Li/H}]_\mathrm{p} = (2.19 \pm 0.28) \times 10^{-10}, \tag{2.48}$$
$$[^7\mathrm{Li/H}]_\mathrm{p} = (2.34 \pm 0.32) \times 10^{-10}, \tag{2.49}$$
$$[^7\mathrm{Li/H}]_\mathrm{p} = (1.26 \pm 0.26) \times 10^{-10}, \tag{2.50}$$

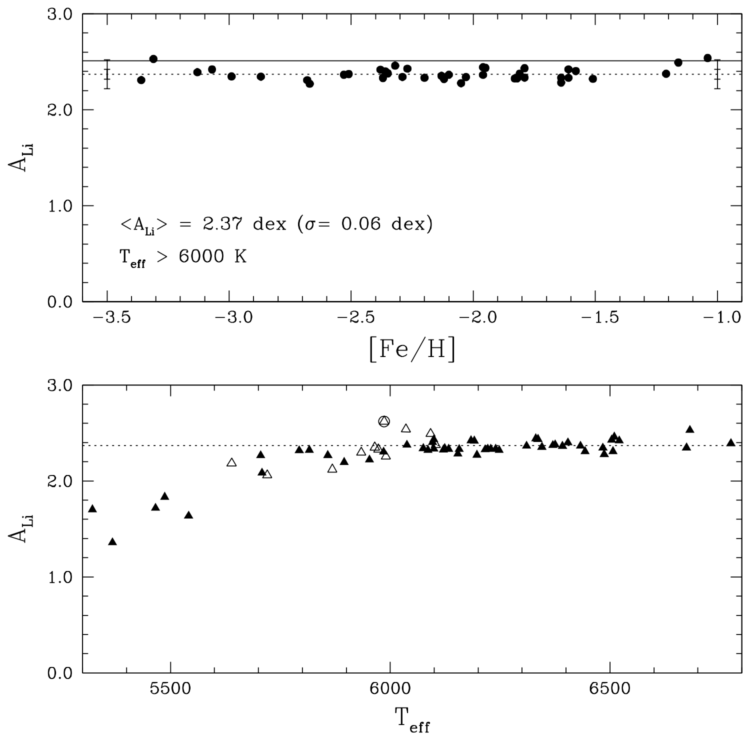

Figure 2.4: Upper panel: $A_{\rm Li}$ of the Spite plateau stars ($T_{\rm eff}$ > 6000K) as a function of [Fe/H]. The dotted line indicates the mean ^7Li abundance of the plateau stars, and the solid line represents the lower limit imposed by the WMAP constraint. The error bars are the predicted error, $\sigma_{\rm pred}$ ($= 10^{0.05} \simeq 1.12$), and $3\sigma_{\rm pred}$ ($= 10^{0.15} \simeq 1.41$). Lower panel: $A_{\rm Li}$ as a function of $T_{\rm eff}$ for stars with [Fe/H] ≤ -1.5 (filled triangles) and [Fe/H] > -1.5 (open triangles). The star (HD106038) with the highest Li abundance (open triangle inside the open circle) is a star with peculiar abundances [45]. This figure is from Ref. [6].

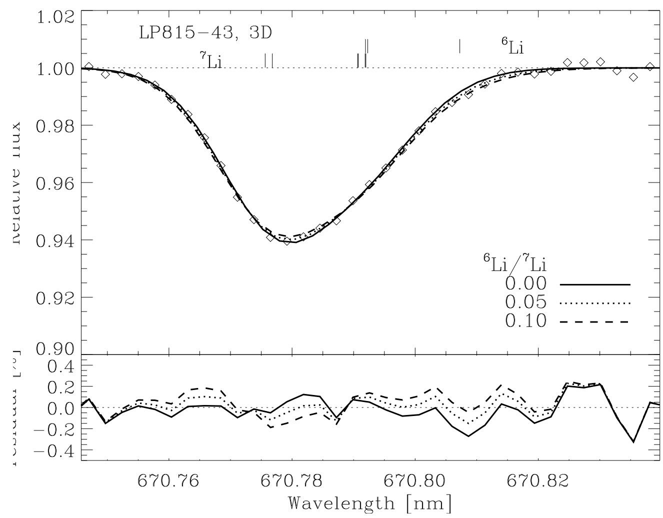

Figure 2.5: The squares indicate the observed date for a star LP 815–43 which has atmospheric parameters $T_{\rm eff}$ = 6400K and [Fe/H] = −2.74. The solid, dotted and dashed line correspond to the best-fitting 3D local thermodynamic equilibrium profile from a χ^2 analysis for ^{6}Li/^{7}Li = +0.00, +0.05 and +0.10, respectively. This figure is from Ref. [48].

(2.48), (2.49) and (2.50) are from Refs. [5], [6] and [47], respectively. Difference between these results is due to systematic error. These results depend on (1) a physical technique to determine the temperature of the stellar atmosphere in which the ^{7}Li absorption line is formed, (2) uncertain inner structure of stars.

In Fig. 2.2 relatively wide error range is taken,

$$[^7\mathrm{Li/H}]_\mathrm{p} = (1.7 \pm 0.02^{+1.1}_{-0}) \times 10^{-10} \tag{2.51}$$

We will, however, use more strictly constrained value (2.50) in the following chapters.

2.3.5 ^{6}Li

^{6}Li is observed in the same source of ^{7}Li. However the observation of ^{6}Li is more difficult than that of ^{7}Li. The absorption line of ^{6}Li is almost hidden in of ^{7}Li since the difference of wavelengths of the lines is only 0.16Å and the strength of ^{6}Li line is 20 times weaker than of ^{7}Li. The presence of ^{6}Li is detected only by slight extra depression of the red wing of the unresolved ^{7}Li feature (see Fig. 2.5 which is from Ref. [48]). In Fig. 2.5 the squares indicate the observed date for a star LP 815–43 which has atmospheric parameters $T_{\rm eff}$ = 6400K and [Fe/H] = −2.74. The solid, dotted and dashed lines correspond to the best-fitting 3D local thermodynamic equilibrium profile from a χ^2 analysis for ^{6}Li/^{7}Li = +0.00, +0.05 and +0.10, respectively.

We thus obtain the primordial abundance of ^{6}Li,

$$^6\mathrm{Li}/^7\mathrm{Li} < 0.046 \pm 0.022. \tag{2.52}$$

2.4 The ^{7}Li problem

As we can see from Fig. 2.2, the predicted abundances based on baryon-to-photon ratio by the WMAP experiment [1] are coincident with observed ones, except for ^{7}Li. The predicted ^{7}Li abundance is

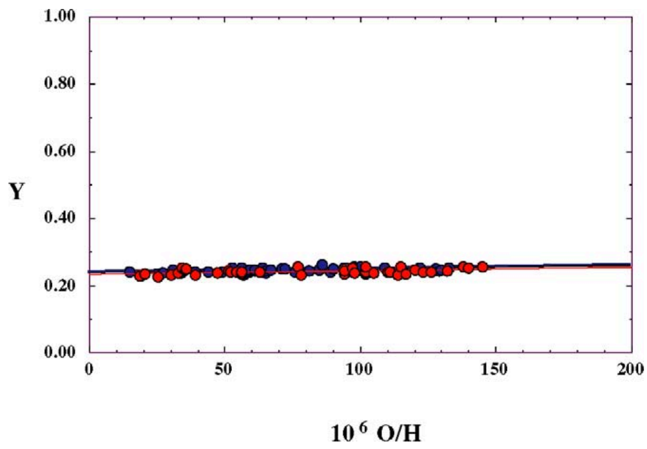

Figure 2.6: The change of the abundance of ^{4}He with the abundance of O. The abundance of ^{4}He is nearly constant and does not fall below about 23 %. This figure is from [33]).

$4.15^{+0.49}_{-0.45} \times 10^{-10}$ as shown in Eq. (2.34), while observed one is $(1.26 \pm 0.26) \times 10^{-10}$ as shown in Eq. (2.50). Therefore the prediction of the BBN gives three times larger abundance than the observation.

Someone might consider that the BBN is wrong in the first place. However the BBN is reliable since the origin of the abundances of ^{4}He and D are well explained by the BBN. The abundance of ^{4}He change with metallicity very little and does not fall below about 23 % as shown in Fig. 2.6 which is from [33]. In particular even in systems with extremely low value of oxygen, which traces stellar activity, the abundance of ^{4}He is nearly constant. This is very different from all other elements, e.g. nitrogen. The abundance of nitrogen goes to zero, as of oxygen goes to zero (see Fig. 2.7 which is from [33]). The abundance of D is not produced any stellar source. Stars destroy deuterium, while no astrophysical site is known for the production of significant amounts of deuterium [49, 50, 51]. Thus abundance of D should be from the BBN.

The inconsistency between observed and predicted values might be explained by poor knowledge of the internal constitution of stars. The quoted observed value is led by an assumption of that the Li abundance in the stellar sample reflects the primordial abundance. However the value might have been affected by convection and/or diffusion in stars. ^{7}Li on the surface of stars are carried into deeper part of the stars by its convection. Normally it is believed that the convention for the hot ($T \gtrsim 5700$K) stars does not affect and the "Spite plateau" is formed since for the hotter stars (i.e. larger stars) the convection layer becomes relatively thin, and stars with temperature $T \gtrsim 5700$K convection layer does not reach the center of the stars. If we adopt unusual model of internal constitution of stars the convection layer can reach the center and the ^{7}Li are reduced. Moreover the ^{7}Li abundance on the surface of stars might be reduced by diffusion. The heavy element diffuse for the center of the star. Diffusion more actively occurs in hotter stars as we can find from the case of Fe (see upper panel of Fig. 2.8 which is from [9]). The ^{7}Li abundance be maximum for the stars with $T \sim 5700$K, and decrease for $T > 5700$K (see lower panel of Fig. 2.8 which is from [9]). Therefore the abundances for $\gtrsim 6000$K is not primordial one but also reduced one. However the effects of convection and diffusion should depend on features of each star. For example the rotation and magnetic field of stars suppress the convection since the tension of the magnetic field line and the repulsion force of the vortex line hold the shape of each line and the convection [53]. The effect of the convection should vary according to each star, and thus conflict with that observed abundance converge with a value (see Fig. 2.4).

The model uncertainty of the stellar atmosphere might explain the discrepancy. We do not observe

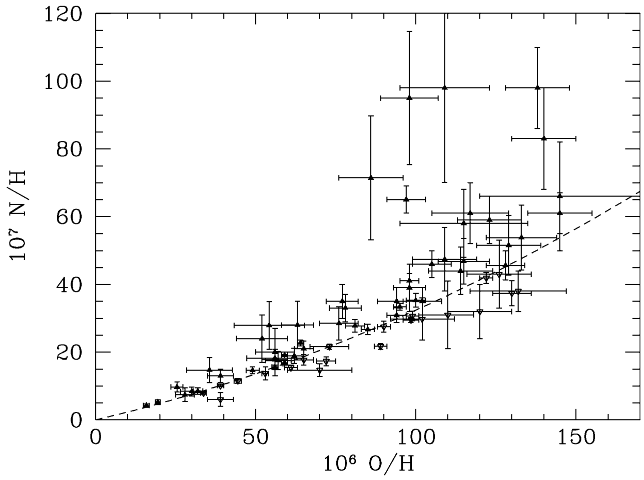

Figure 2.7: The change of the abundance of N with the abundance of O. The abundance of N goes to zero according to O. This figure is from [33]).

^{7}Li directly but absorption line of stellar atmosphere. The determination of the strength of the line depends on models and the surface temperature via some physical parameters, e.g. surface gravity. The uncertainty of the surface temperature is up to 150–200K and can lead to an underestimation of up to $10^{0.09} \simeq 1.23$. However this modification is not enough to the discrepancy.

Another possible explanation is uncertainty of nuclear reaction rates. The uncertainty of nuclear reactions rate of ^{7}Li reduction processes;

$$^7\mathrm{Li} + \mathrm{D} \to n + 2^4\mathrm{He}, \tag{2.53}$$

$$^7\mathrm{Be} + \mathrm{D} \to p + 2^4\mathrm{He}, \tag{2.54}$$

is bigger than of D, ^{3}He and ^{4}He. Nevertheless the uncertainty is not enough to resolve the discrepancy [2]. Further the uncertainty of ^{7}Li reduction processes;

$$^3\mathrm{He} + {}^\mathrm{H}\mathrm{e} \to \gamma + {}^7\mathrm{Be} \tag{2.55}$$

is strictly constrained by the combination of standard solar model and neutrino experiment [54].

Thus we conclude that the ^{7}Li problem is not resolved in the SM. An interesting approach to this problem is given by effects induced by new physics beyond the SM. Exotic particles which have long lifetime and interact with nuclei might give a solution to the ^{7}Li problem since they survive until the BBN era and open new channels to reduce the nuclei. In the minimal supersymmetric standard model (MSSM) with the conservation of R-parity, such a long lived and interacting particle can appear and give the solution. It is a superpartner of tau lepton, stau. In the next chapter we see the nature of stau and check the possibility to solve the ^{7}Li problem.

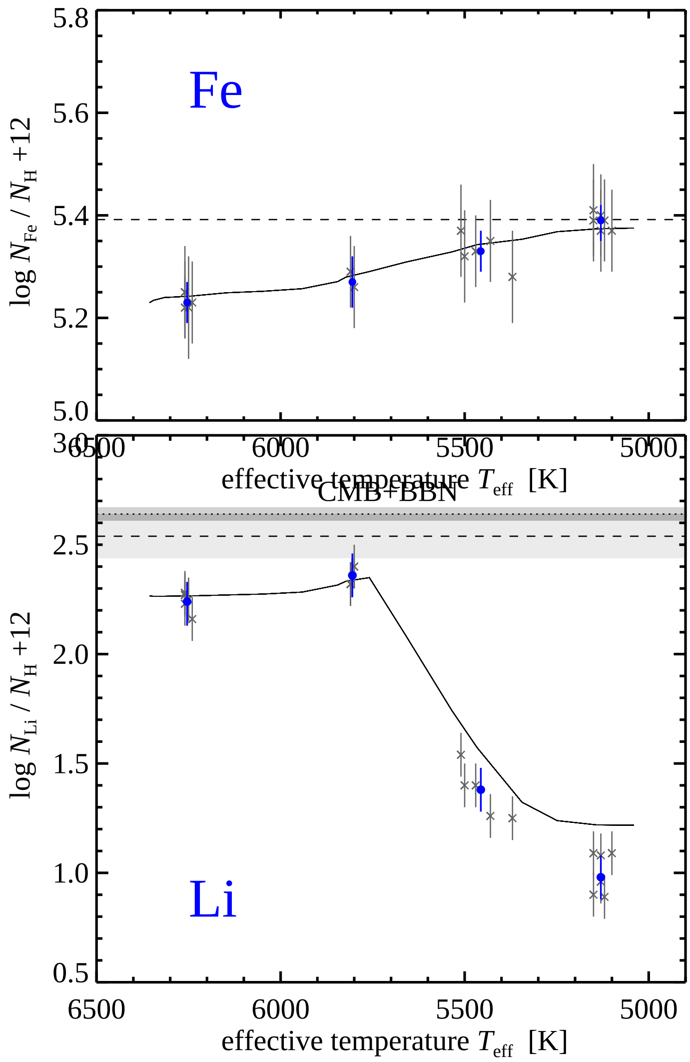

Figure 2.8: Temperature change of iron and lithium of the observed stars compared to the model predictions. The gray crosses are the individual measurements, while the blue circle are the group averages. The solid lines are the predictions of the diffusion model[52], with the original abundance given by the dashed line. In lower panel, the shaded area around the dotted line indicates the 1σ confidence interval of CMB + BBN[1]: $\log(N_{\rm Li}/N_{\rm H})+12 = 2.64 \pm 0.03$. For iron, the error bars are the line-to-line scatter of FeI and FeII (propagated into the mean for the group averages), whereas for the absolute lithium abundances 0.10 is adopted. The 1σ confidence interval around the inferred primordial lithium abundance ($\log(N_{\rm Li}/N_{\rm H}) + 12 = 2.54 \pm 0.10$) is indicated by the light-gray area. These figures are from [9].

Chapter 3

Stau

In this chapter we investigate the decay of the stau. First we briefly consider the reason for the existence of the stau. Next we investigate the decay process of the stau and its decay rate. We will find that staus can be long lived and couple with hadronic current, enough to solve the ^{7}Li problem.

3.1 Dark matter and supersymmetry

The existence of non-baryonic dark matter is now confirmed and its density has been quantitatively estimated [55, 56]. However its identity is still unknown. One of the most prominent candidates is the weakly interacting massive particle (WIMP) [57, 58, 59, 60].

As is well known, the supersymmetric extension of the Standard Model provides a stable exotic particle, the lightest supersymmetric particle (LSP), if R parity is conserved. Among LSP candidates, the neutralino LSP is the most suitable for non-bar ionic dark matter since its nature fits that of the WIMP [61, 62]. Neutralinos are a linear combination of the supersymmetric partners of the U(1) and SU(2) gauge bosons (bino and wino) and the Higgs bosons (Higgsino). They have mass in a range from 100 GeV to several TeV and are electrically neutral. The lightest neutralino is stable if R parity is conserved.

Since the supersymmetric extension of the Standard Model is the most attractive theory, the nature of neutralino dark matter has been studied extensively [63]. In many scenarios of the supersymmetric model, the LSP neutralino consists mainly of the bino, the so-called bino-like neutralino. In this case, naive calculations show that the predicted density in the current universe is too high and it is necessary to find a way to reduce it. One mechanism to suppress the density is coannihilation [64]. If the next lightest supersymmetric particle (NLSP) is nearly degenerate in mass with the LSP, the interaction of the LSP with the NLSP is important in calculating the LSP annihilation process. For coannihilation to occur tight degeneracy is necessary, since without coannihilation the LSP decouples from the thermal bath at $T \sim m/20$ [65], where m is the LSP mass. Therefore the mass difference δm must satisfy $\delta m/m <$ a few %, otherwise the NLSP decouples before coannihilation becomes dominant. Furthermore, if the degeneracy is much tighter, we would observe a line spectrum of photons from pair annihilation of dark matter [66, 67], since the annihilation cross section of dark matter would be strongly enhanced due to the threshold correction.

A candidate for the NLSP is the stau or stop in many class of MSSM, and in this paper we study the lifetime of the stau-like slepton having mass degenerate with the LSP neutralino. For the neutralino LSP to be dark matter, very tight degeneracy is required in mass between the NLSP and the LSP neutralino. In particular the heavier the LSP is, the tighter the degeneracy must be [63]. For such a degeneracy, the NLSP is expected to have a long lifetime due to phase space suppression [68, 69].

An alternative scenario for a long-lived scalar particle is the gravitino LSP. Considerable work has been devoted to the long life NLSP in the context of the gravitino LSP. In this case, due to the small coupling between a superWIMP (including the gravitino) and the NLSP, the lifetime of the NLSP becomes very long [70, 71, 72]. To determine the most likely candidate for the LSP, we can accumulate and identify [73, 74] the candidate for long-lived NLSPs and compare the nature of the particles including couplings. In this thesis we concentrate in neutralino LSP scenario.

3.2 Decay rate

In this section, we calculate the decay rate of the stau NLSP. The stau is a mass eigenstate consisting of superpartners of left- and right-handed taus,

$$\tilde{\tau} = \cos\theta_\tau \tilde{\tau}_L + \sin\theta_\tau e^{-i\gamma_\tau}\tilde{\tau}_R. \tag{3.1}$$

Here, θ_τ is the mixing angle between $\tilde{\tau}_L$ and $\tilde{\tau}_R$, and γ_τ is the CP violating phase. The decay mode is governed by the mass difference, $\delta m \equiv m_{\rm NLSP} - m_{\rm LSP}$, according to kinematics. That is, the lifetime of the stau depends strongly on δm.

We consider the following four decay modes,

$$\tilde{\tau} \to \tau\tilde{\chi}^0, \tag{3.2}$$
$$\tilde{\tau} \to \pi\nu_\tau\tilde{\chi}^0, \tag{3.3}$$
$$\tilde{\tau} \to l\nu_l\nu_\tau\tilde{\chi}^0, \tag{3.4}$$

where l denotes electron, e, and muon, μ, but not tau lepton (see Fig. 3.1). Note that the NLSP can decay into other particles, for example, if $\delta m > 1.86$ GeV, a D meson can be produced in the stau decay but $\tilde{\tau} \to \tilde{\chi}^0\tau$ is dominant in this δm region since the D meson production process is suppressed by couplings and propagators. In the 3-body and 4-body decay processes, $\tilde{\tau} \to \tilde{\chi}^0\nu_\tau\pi$, $\tilde{\tau} \to \tilde{\chi}^0\mu\nu_\tau\nu_\mu$, and $\tilde{\tau} \to \tilde{\chi}^0 e\nu_\tau\nu_e$, diagrams can be formulated with charginos as intermediate states, however, such processes are strongly suppressed by the chargino propagator and we can safely ignore them [68].

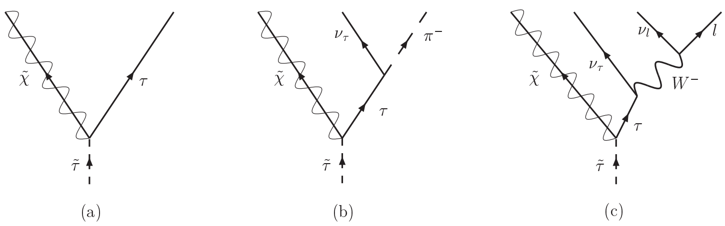

Figure 3.1: Feynman diagrams of stau decay: (a) $\tilde{\tau} \to \tilde{\chi}^0\tau$, (b) $\tilde{\tau} \to \tilde{\chi}^0\nu_\tau\pi$, (c) $\tilde{\tau} \to \tilde{\chi}^0 l\nu_\tau\nu_l$.

In this paper, we consider the small mass difference case and hence we can ignore the momentum in the W boson propagator. Thus the interaction Lagrangian is given by

$$\mathcal{L}_{int} = \tilde{\tau}^* \bar{\tilde{\chi}}^0(g_L P_L + g_R P_R)\tau + \frac{G}{\sqrt{2}}\nu_\tau\gamma_\mu P_L\tau J^\mu + \frac{4G}{\sqrt{2}}(\bar{l}\gamma^\mu P_L\nu_l)(\bar{\nu}_\tau\gamma_\mu P_L\tau) + h.c. \tag{3.5}$$

The first term describes stau decay into a neutralino and a tau. Here, P_L and P_R are the projection operators and g_L and g_R are the coupling constants given by, for example in the bino-like neutralino case,

$$g_L = \frac{g}{\sqrt{2}\cos\theta_W}\sin\theta_W\cos\theta_\tau, \quad g_R = \frac{\sqrt{2}g}{\cos\theta_W}\sin\theta_W\sin\theta_\tau e^{i\gamma_\tau}, \tag{3.6}$$

where g is the weak coupling constant and θ_W is the Weinberg angle. The second and third terms describe tau decays into a pion and/or leptons, where G is the Fermi constant.

The detailed calculation of the stau decay rate is given in the appendix A. Here we show approximate formulae. In the region $\delta m > m_\tau$, 2-body decay (see Fig. 3.1(a)) is allowed kinematically and is dominant. The decay rate of the 2-body final state is approximately

$$\Gamma_{\text{2-body}} = \frac{1}{4\pi m_{\tilde{\chi}^0}}\sqrt{(\delta m)^2 - m_\tau^2}\left((g_L^2 + |g_R|^2)\delta m - 2Re[g_L g_R]m_\tau\right) \ , \tag{3.7}$$

where $m_{\tilde{\tau}}, m_{\tilde{\chi}^0}$, and m_τ are the masses of $\tilde{\tau}$, $\tilde{\chi}^0$, and τ, respectively.

The 2-body decay is forbidden kinematically for $\delta m < m_\tau$, and pion production (see Fig. 3.1(b)) is dominant if δm is larger than the pion mass m_π. The pion production 3-body decay rate has the approximate form

$$\begin{aligned}\Gamma_{\text{3-body}} = &\frac{G^2 f_\pi^2\cos^2\theta_c}{210(2\pi)^3 m_{\tilde{\chi}^0} m_\tau^4}\left((\delta m)^2 - m_\pi^2\right)^{5/2} \\ &\times\left[g_L^2\delta m\left(4(\delta m)^2 + 3m_\pi^2\right) - 2Re[g_L g_R]m_\tau\left(4(\delta m)^2 + 3m_\pi^2\right) + 7|g_R|^2 m_\tau^2\delta m\right] .\end{aligned} \tag{3.8}$$

Here f_π is the pion decay constant and θ_c is the Cabbibo angle.

Incidentally, we note that a quark cannot appear alone in any physical processes, a point that was missed in ref. [68]. Hence, u and d quarks appear only as mesons and the u, d production process is relevant only for $\delta m > m_\pi$.

Finally, when the mass difference is smaller than the pion mass, 4-body decay processes, $\tilde{\tau} \to \tilde{\chi}^0\mu\nu_\tau\nu_\mu$ and $\tilde{\tau} \to \tilde{\chi}^0 e\nu_\tau\nu_e$, are significant (see Fig. 3.1(c)). The approximate decay rate is calculated as

$$\begin{aligned}\Gamma_{\text{4-body}} = &\frac{G^2}{945(2\pi)^5 m_{\tilde{\chi}^0} m_\tau^4}\left((\delta m)^2 - m_l^2\right)^{5/2} \\ &\times\Big[2g_L^2(\delta m)^3\left(2(\delta m)^2 - 19m_l^2\right) - 4Re[g_L g_R]m_\tau(\delta m)^2\left(2(\delta m)^2 - 19m_l^2\right) \\ &\quad + 3|g_R|^2 m_\tau^2\delta m\left(2(\delta m)^2 - 23m_l^2\right)\Big] .\end{aligned} \tag{3.9}$$

Here m_l is the charged lepton (e or μ) mass.

3.3 Parameter dependence

In this section, we discuss the parameter dependence of the stau lifetime and the cosmological constraints for the parameters in the bino-like LSP case. From Eqs. (3.7), (3.8), and (3.9), we see that the stau lifetime depends on $\delta m, \theta_\tau, m_{\tilde{\chi}^0}$, and γ_τ.

3.3.1 $m_{\tilde{\chi}}$

First, we examine the neutralino mass dependence of the lifetime. We consider the cosmological constraints for dark matter to get the mass range of the LSP. It is well known that the dark matter relic density is reduced by the coannihilation process and hence the neutralino mass can be heavier than it would be without coannihilation. Accounting for the coannihilation process gives a neutralino mass range (the first ref. of [63]) of

$$200 \text{ GeV} \leq m_{\tilde{\chi}} \leq 600 \text{ GeV}. \tag{3.10}$$

Here, we use CMSSM bound as a reference value of $m_{\tilde{\chi}}$, though we study the stau lifetime in general MSSM framework, since it is not strongly dependent on $m_{\tilde{\chi}}$ as noted below. This is consistent with the cosmological constraint, $0.094 \leq \Omega_{DM} h^2 \leq 0.129$.

It is clear from Eqs. (3.7), (3.8), and (3.9) that the stau lifetime is proportional to the neutralino mass. We can see it also from figures 3.2(a)–(c), where we set $\delta m = 0.01$GeV, $\theta_\tau = \pi/3$ and $\gamma_\tau = 0$, and $\delta m = 0.01$GeV for 3.2(a), $\delta m = 0.5$GeV for 3.2(b) and $\delta m = 2.0$GeV for 3.2(c). Therefore in the mass range given in Eq. (3.10), the stau lifetime varies by a factor of three. Taking this into account, we use only $m_{\tilde{\chi}} = 300$GeV in our figures.

3.3.2 δm

Next, we consider the δm dependence of the stau lifetime. For coannihilation to occur, the mass difference must satisfy $\delta m / m_{\tilde{\chi}^0} \sim$ a few % or smaller [64]. Therefore, δm must be smaller than a few GeV. The δm dependence of the total stau lifetime and the partial lifetimes of each decay mode in this δm region is shown in Fig. 3.3. In Fig. 3.3, we set the values as follows: $m_{\tilde{\chi}^0} = 300$ GeV, $\theta_\tau = \pi/3$, and $\gamma_\tau = 0$.

From Fig. 3.3, we can see which mode is dominant for a certain δm. The figure shows that the lifetime increases drastically as δm becomes smaller than the tau mass. This is because taus are produced in the region $\delta m > m_\tau$, while in the region $\delta m < m_\tau$, taus cannot be produced and instead pions appear in the final state. At $\delta m = m_\pi$ the lifetime increases slightly. This is due to the fact that the dominant mode changes from 3-body to 4-body decay. In contrast, at $\delta m = m_\mu$ the lifetime does not increase much, even though above this mass, muons can be created. This is because at the pion mass, the muon production process is already kinematically suppressed and the electron production process governs the stau decay.

To understand the δm dependence of the lifetime quantitatively and intuitively we determine the power of δm in the decay rate, considering stau decay into neutralino and $n-1$ massless particles. The δm dependence of the decay rate is determined by the phase space and the squared amplitude [68].

First, we examine the δm dependence by considering the phase space. For 2-body decay, a phase space consideration gives

$$d\phi^{(2)} = \frac{d\Omega}{32\pi^2} \left(1 - \left(\frac{m_{\tilde{\chi}^0}}{m_{\tilde{\chi}^0} + \delta m} \right)^2 \right) \propto \delta m \ . \tag{3.11}$$

By using a recursion relation between $d\phi^{(n)}$ and $d\phi^{(n-1)}$, the phase space of n-body decay renders the δm dependence as

$$\begin{aligned} d\phi^{(n)} &\propto d\phi^{(n-1)} \times \int^{\delta m} d\mu (d\phi^{(2)}) \\ &\propto (\delta m)^{2(n-2)+1} \ . \end{aligned} \tag{3.12}$$

Second, we consider the δm dependence from the squared amplitude. If all of the $n-1$ massless particles are fermions, the squared amplitude depends on δm as

$$\mathcal{M}^{(n)} \propto (\delta m)^{n-1} \ , \tag{3.13}$$

since it depends linearly on the massless fermion momentum. Thus, we obtain the dependence of the

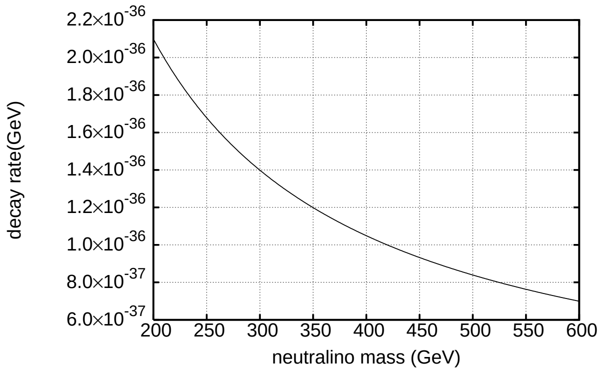

(a)

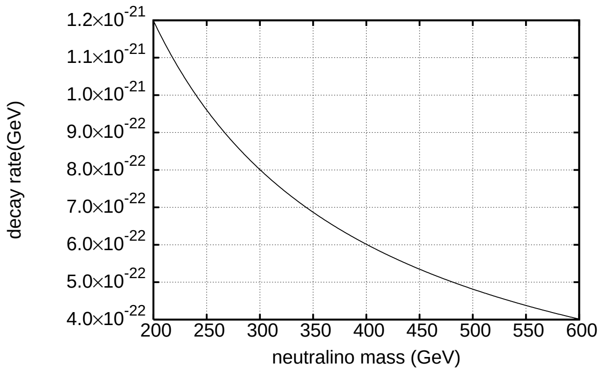

(b)

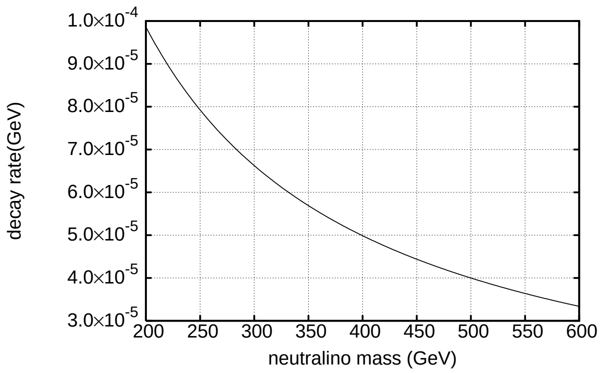

(c)

Figure 3.2: Neutralino mass and stau lifetime. We set $\delta m = 0.01$GeV, $\theta_\tau = \pi/3$ and $\gamma_\tau = 0$, and $\delta m = 0.01$GeV for 3.2(a), $\delta m = 0.5$GeV for 3.2(b) and $\delta m = 2.0$GeV for 3.2(c).

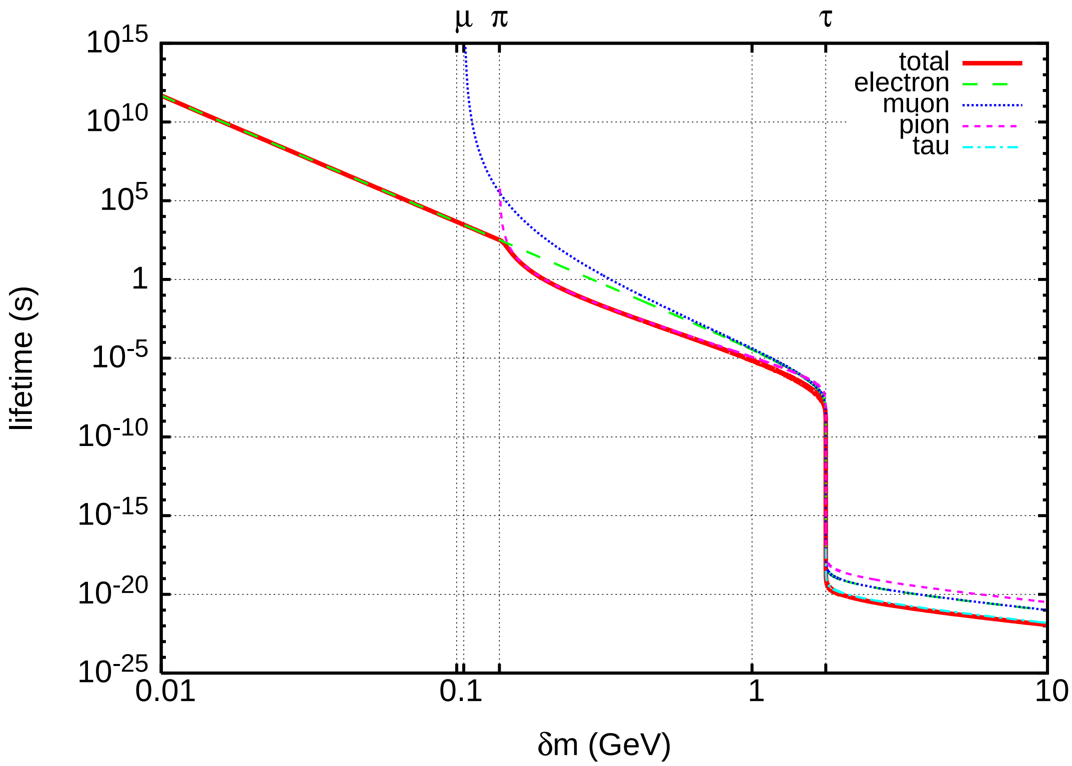

Figure 3.3: Total lifetime and partial lifetimes of each decay mode as a function of δm. The lines label electron, muon, pion, and tau correspond to the processes $\tilde{\tau} \to \tilde{\chi}^0 e \nu_\tau \nu_e$, $\tilde{\tau} \to \tilde{\chi}^0 \mu \nu_\tau \nu_\mu$, $\tilde{\tau} \to \tilde{\chi}^0 \nu_\tau \pi$, and $\tilde{\tau} \to \tilde{\chi}^0 \tau$, respectively. Here we take $m_{\tilde{\chi}^0} = 300$ GeV, $\theta_\tau = \pi/3$, and $\gamma_\tau = 0$.

decay rate on δm for a final state of only fermions,

$$\Gamma^{(n)} \propto \mathcal{M}^{(n)} \times d\phi^{(n)} \propto (\delta m)^{3n-4} . \tag{3.14}$$

In contrast, if one pion(NG-boson) appears in the stau decay process, the δm dependence of the squared amplitude becomes

$$\mathcal{M}^{(n)} \propto (\delta m)^{n} . \tag{3.15}$$

This change in the decay process is due to the fact that the amplitude of the pion production is proportional to the pion momentum. Namely, the squared amplitude of the pion production process is proportional to the pion momentum squared. Thus the δm dependence of the process, in which one pion is involved, is

$$\Gamma^{(n)} \propto (\delta m)^{3(n-1)} . \tag{3.16}$$

In the massless limit of external line particles, the δm dependences of our results, calculated in appendix A, are

$$\begin{aligned} \Gamma_{\text{2-body}} &\propto (\delta m)^2, \\ \Gamma_{\text{3-body}} &\propto (\delta m)^6, \\ \Gamma_{\text{4-body}} &\propto (\delta m)^8 \ , \end{aligned} \tag{3.17}$$

which are consistent with Eq. (3.14) and Eq. (3.16).

More precisely, by taking into account the masses of the produced particles, we get the complicated δm dependences

$$\begin{aligned}
\Gamma_{\text{2-body}} &\propto (\delta m)\left((\delta m)^2 - m_\tau^2\right)^{1/2}, \\
\Gamma_{\text{3-body}} &\propto (\delta m)^{-2}\left((\delta m)^2 - m_\pi^2\right)^{7/2}, \\
\Gamma_{\text{4-body}} &\propto (\delta m)^{3}\left((\delta m)^2 - m_l^2\right)^{5/2}.
\end{aligned} \tag{3.18}$$

These equations clearly show the δm dependence of the stau lifetime.

3.3.3 γ_τ

We next consider the γ_τ dependence of the stau lifetime. Figures 3.4(a)–3.4(c) show the lifetime as a function of the CP violating phase. We set $m_{\tilde{\chi}} = 300\text{GeV}$ and $\theta_\tau = \pi/3$ for all these figures. On the other hand we set $\delta m = 0.01\text{GeV}$ for Figure 3.4(a), $\delta m = 0.5\text{GeV}$ for Figure 3.4(b) and $\delta m = 2\text{GeV}$ for Figure 3.4(c).

From Figs. 3.4(a)–3.4(c), it is clear that the CP violating phase does not greatly affect the stau lifetime, and so we fix $\gamma_\tau = 0$ (no CP violation).

As expressed in Eq. (3.9), the effect of CP violation appears in the $Re[g_L g_R]$ terms only. Since the coefficients of the $Re[g_L g_R]$ terms are smaller than those of $|g_R|^2$, it is again clear that the CP violating phase does not greatly affect the stau lifetime.

3.3.4 θ_τ

The θ_τ dependence of the stau lifetime is as strong as the δm dependence. Figures 3.5(a)–3.5(c) show the θ_τ dependence of the stau lifetime. We set $m_{\tilde{\chi}} = 300\text{GeV}$ and $\gamma_\tau = 0$ for all these figures, and $\delta m = 0.01$ GeV for 3.5(a), and $\delta m = 0.5$ GeV for 3.5(b) and and $\delta m = 2.0$ GeV for 3.5(c).

We can see from Fig. 3.5(a) that for $\delta m \ll m_\tau$, $\tilde{\tau}_R$ decays much more quickly than $\tilde{\tau}_L$. This can be understood by considering two steps. First, we note that only left-handed virtual taus contribute to the final state ν_τ. Second, $\tilde{\tau}_R$ converts to τ_L by picking up m_τ in the tau propagator, while $\tilde{\tau}_L$ converts by picking up the momentum p_τ in the propagator.

Since $p_\tau \sim \delta m \ll m_\tau$, the former contribution is much larger and hence there is a strong dependence on θ_τ.

3.4 Lepton flavor violation

We next consider Lepton flavor violation (LFV)*. The NLSP slepton might be a linear combination of flavor eigenstates. It is expected that lepton flavor violating events will be observed due to this mixing, such as $\mu \to e\gamma$. If we observe $\tau \to e\gamma$ or $\tau \to \mu\gamma$ events, then within the context of the minimal supersymmetric Standard Model (MSSM), we would conclude that the selectron forms part of the NLSP:

$$\phi_{\text{NLSP}} = N_1 \tilde{e} + \sqrt{1 - N_1^2}\,\tilde{\tau}. \tag{3.19}$$

The branching ratio of $\tau \to e\gamma$ is roughly proportional to N_1^2. The current upper bound on the branching ratio, $< O(10^{-7})$, gives a poor constraint, at most $N_1 < 0.1$. If $N_1 \neq 0$, the NLSP slepton can decay,

$$\phi_{\text{NLSP}} \to \tilde{\chi} + e, \tag{3.20}$$

*For the ref. of superWIMP case, see for example[71]

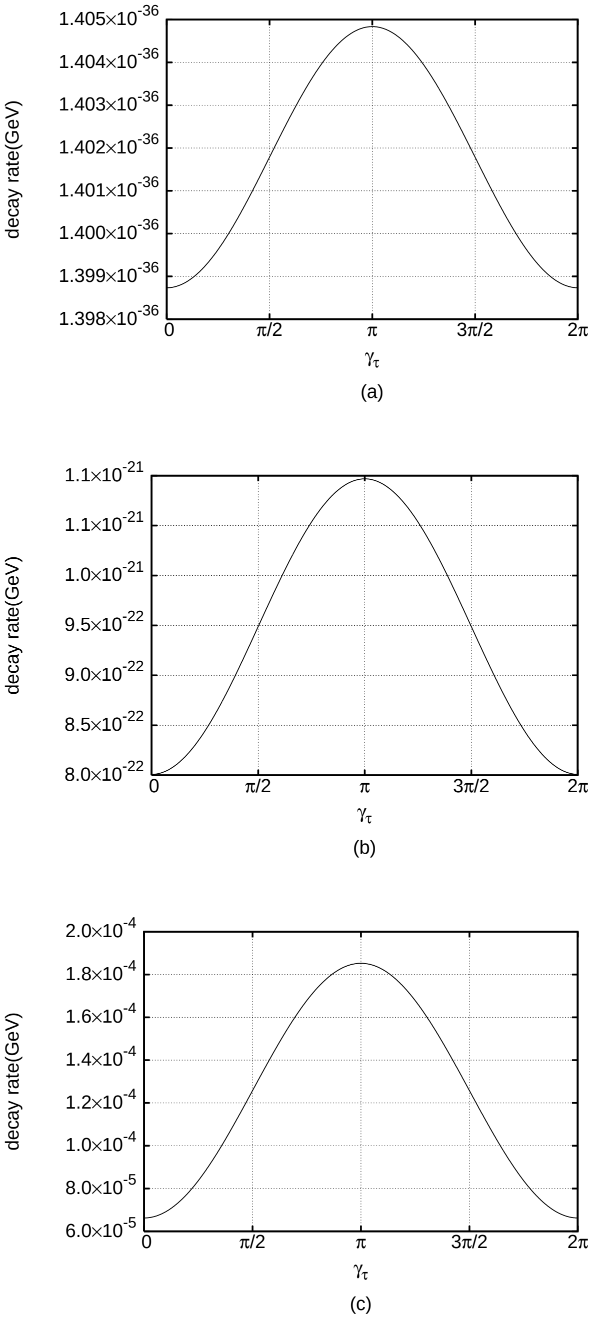

Figure 3.4: CP violating phase and stau lifetime. we set $m_{\tilde{\chi}} = 300\mathrm{GeV}$ and $\theta_\tau = \pi/3$, and $\delta m = 0.01\mathrm{GeV}$ for Figure 3.4(a), $\delta m = 0.5\mathrm{GeV}$ for Figure 3.4(b) and $\delta m = 2\mathrm{GeV}$ for Figure 3.4(c).

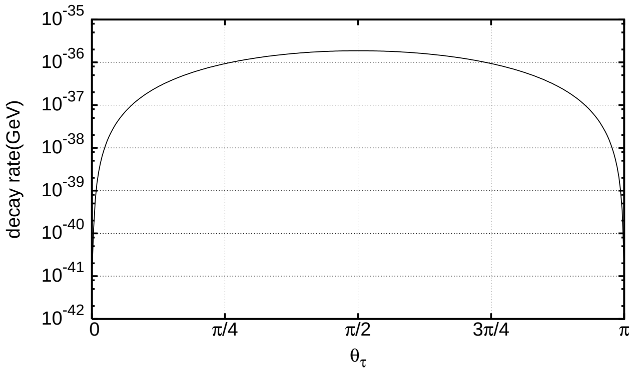

(a)

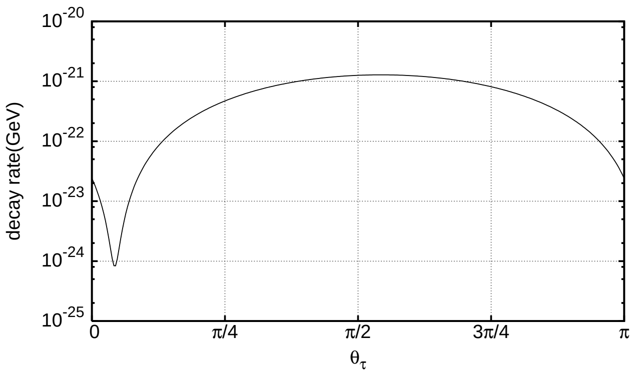

(b)

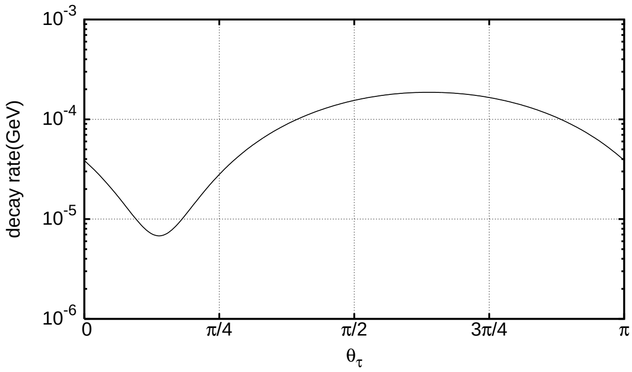

(c)

Figure 3.5: Stau mixing angle and stau lifetime. We set $m_{\tilde{\chi}} = 300\text{GeV}$ and $\gamma_\tau = 0$ for all these figures, and $\delta m = 0.01$ GeV for 3.5(a), and $\delta m = 0.5$ GeV for 3.5(b) and and $\delta m = 2.0$ GeV for 3.5(c).

with a lifetime of

$$1.666 \times 10^{-18} \left(\frac{m_{\tilde{\chi}^0}}{300\text{GeV}} \right) \left(\frac{1.0\text{GeV}}{\delta m} \right)^2 \left(\frac{0.1}{N_1} \right)^2 \text{sec} \ . \tag{3.21}$$

If $N_1 \gtrsim 10^{-10}$ staus has shorter lifetime than 1 sec and can not survive until the big-bang nucleosynthesis era. We, however, ignore the possibility of existence of LFV in this thesis.

3.5 Connection with the Big-Bang Nucleosynthesis

In the last section we saw that the processes (3.2), (3.3) and (3.4) have typical lifetimes $\mathcal{O}(10^{-20})$sec, $(10^{-6} - 10^{2})$ sec, and $(10^{2} - 10^{12})$ sec, respectively. Since the BBN takes place $(1 - 100)$ sec after the big-bang, the staus will decay entirely before the BBN unless the channel (3.2) is closed. On the other hand it is possible that the staus solve the ^{7}Li problem when $\delta m \lesssim \mathcal{O}(100)$MeV. Note that the channel (3.3) also closes when δm is less than the pion mass $m_\pi \simeq 140$ MeV. Although the required LSP-NLSP mass difference is small compared to the typical mass of LSP which is $\mathcal{O}(100\,\text{GeV})$, it is preferable in attributing the dark matter (DM) to the neutralino LSPs since it allows the LSP-NLSP coannihilation. With this tiny δm, the neutralino naturally becomes a cold dark matter instead of warm or hot dark matter [75] even though it is produced non-thermally. Hence our model is free of the constraints from the large-scale structure formation of the universe.

Chapter 4

Destruction of nuclei by the stau

In the last chapter we saw that staus have attractive features for the destruction of ^{7}Be and ^{7}Li, or collectively ^{7}Be/^{7}Li; (1) interactions with stau are of beyond the SM and can modify the result of SBBN, (2) as we see below staus interact with nuclei since they couple with the hadronic current J^μ, (3) staus can be long lived and abundant at the time of BBN when the staus and neutralinos have a mass difference tiny enough.

In this chapter we see some interactions between a stau and a nucleus. The interactions introduce additional decay channels of ^{7}Be/^{7}Li to the standard BBN theory. The additional channels give a possible solution to the ^{7}Li problem where the theoretical prediction of the abundance of ^{7}Be/^{7}Li exceeds the observational results by a factor of $\sim$ 2–3. We consider the lifetimes of the process because it is crucial to understand the impact upon the modification of the BBN, and find that interactions induced by stau–nucleus bound states become dominant among the additional channels.

4.1 Hadronic-current interaction with free staus

In this section, we consider a interaction between a free stau and a nucleus caused by a hadronic current exchange. Staus can interact with the nuclei through the hadronic current and thereby alter the BBN processes. The abundances of ^{7}Li/^{7}Be are changed by the new decay channels (see also Fig. 4.1):

$$\tilde{\tau} \to \tilde{\chi}^0 + \nu_\tau + \pi^\pm, \tag{4.1}$$
$$\pi^+ + {}^7\mathrm{Li} \to {}^7\mathrm{Be}, \tag{4.2}$$
$$\pi^- + {}^7\mathrm{Be} \to {}^7\mathrm{Li} \tag{4.3}$$
$$\pi^- + {}^7\mathrm{Li} \to {}^7\mathrm{He}. \tag{4.4}$$

The process $\pi^+ + {}^7\mathrm{He} \to {}^7\mathrm{Li}$ does not occur since ^{7}He is very unstable.

The reaction rate of the interaction $\mathit{\Gamma}_{\text{free stau}}$ is obtained from the Lagrangian (3.5) as

$$\mathit{\Gamma} = n_N \cdot (\sigma v), \tag{4.5}$$

where n_N is the number density of the nucleus, and $N = {}^7$Be for the process (4.17) and $N = {}^7$Li for (4.18). The cross section of the interaction for the process (4.17) is given by,

$$\begin{aligned}(\sigma v) \equiv \frac{1}{2E_{\tilde{\tau}} 2E_{\mathrm{Be}}} \int \mathrm{dLIPS} \left|\langle \tilde{\chi}^0 \nu_\tau {}^7\mathrm{Li} | \mathcal{L}_{\mathrm{int}} | \tilde{\tau} {}^7\mathrm{Be}\rangle\right|^2 \\ \times (2\pi)^4 \delta^{(4)}(p_{\tilde{\tau}} + p_{\mathrm{Be}} - p_{\tilde{\chi}^0} - p_{\nu_\tau} - p_{\mathrm{Li}}),\end{aligned} \tag{4.6}$$

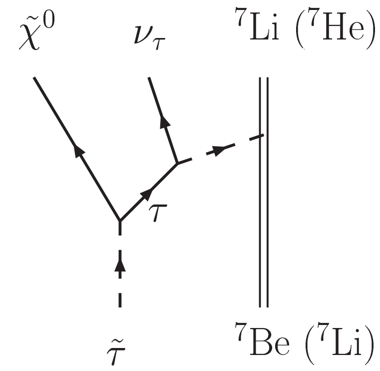

Figure 4.1: Interaction between a free stau and a nucleus caused by a hadronic current exchange.

where

$$\mathrm{dLIPS} = \prod_i \frac{\mathrm{d}^3\boldsymbol{p}_i}{(2\pi)^3 2E_i}. \tag{4.7}$$

Here $i \in \{\tilde{\chi}^0, \nu_\tau, {}^7\mathrm{Li}\}$ for the process (4.17) and $i \in \{\tilde{\chi}^0, \nu_\tau, {}^7\mathrm{He}\}$ for (4.18). $\mathcal{L}_{int}$ is defined in Eq. 3.5. The following approximations are applied to evaluate the reaction rate further. The matrix element appearing in Eq 4.6 is divided into hadronic part and leptonic part,

$$\langle \tilde{\chi}^0 \nu_\tau {}^7\mathrm{Li} | \mathcal{L}_{\mathrm{int}} | \tilde{\tau} {}^7\mathrm{Be} \rangle = \langle {}^7\mathrm{Li} | J_\mu | {}^7\mathrm{Be} \rangle \cdot \langle \tilde{\chi}^0 \nu_\tau | \tilde{\tau}^* \bar{\tilde{\chi}}^0 (g_L P_L + g_R P_R) \tau \cdot \frac{G}{\sqrt{2}} \nu_\tau \gamma^\mu P_L \tau | \tilde{\tau} \rangle \tag{4.8}$$

The hadronic part of the matrix element in Eq. (4.6) is evaluated by the ft-value of the corresponding β-decay obtained from the experiments,

$$\left| \langle {}^7\mathrm{Li} | J_\mu | {}^7\mathrm{Be} \rangle \right|^2 = \frac{16\pi^3 E_{Be} E_{Li} \log 2}{m_e^5 G^2} \frac{1}{ft}, \tag{4.9}$$

(see Appendix B). We note that according with the evaluation by ft-value we neglect the recoil of the nucleus and thus components of the $\mu = 1, 2, 3$. The experimental ft-value is available for ^{7}Li $\leftrightarrow$ ^{7}Be but not for ^{7}Li $\leftrightarrow$ ^{7}He, however. We assume that the two processes have the same ft-value. As long as we consider the quantum numbers of the ground state of ^{7}Li and ^{7}He we can expect a Gamow-Teller transition can take place since they are similar with those of ^{6}He and ^{6}Li and we know that they make a Gamow-Teller transition. The Gamow-Teller transition is superallowed and has a similar ft-value to the Fermi transition such as ^{7}Li $\leftrightarrow$ ^{7}Be.

The inverse of the reaction rate Eq. (4.5) is shown in Fig. 4.2. Here we take same parameters of stau with Fig. 3.3; $m_{\tilde{\chi}^0} = 300$ GeV, $\theta_\tau = \pi/3$ and $\gamma_\tau = 0$. In the region $\delta m \lesssim \mathcal{O}(100)$ MeV which is interested to solve the ^{7}Li problem the inverse rate is ($\mathcal{O}(10^{27})$–$\mathcal{O}(10^{30})$) sec and much longer than the time scale of the BBN. Thus the ^{7}Li problem is not solved by the interaction with free staus.

The ineffectiveness of this process is due to the low density of the ^{7}Li in the universe. Since ^{7}Li/H $\sim$

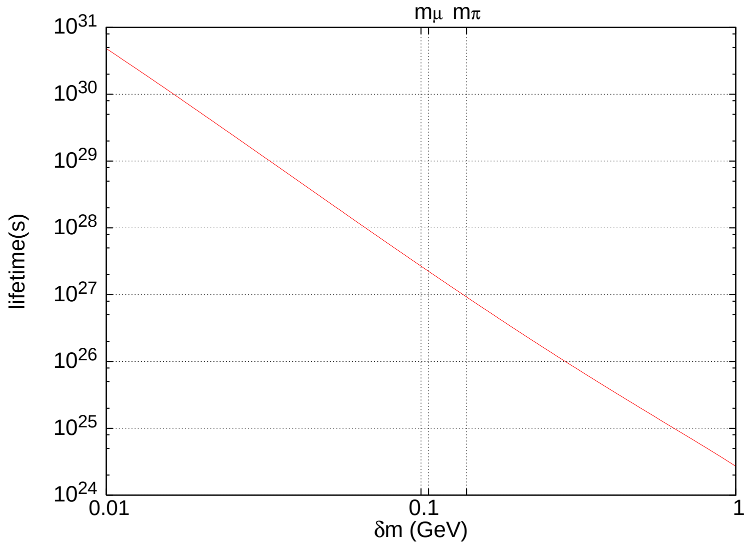

Figure 4.2: The inverse decayrate of hadronic-current interaction with free staus as the function of δm. We take $m_{\tilde{\chi}^0} = 300$ GeV, $\theta_\tau = \pi/3$ and $\gamma_\tau = 0$.

10^{-10} the number density of the ^{7}Li, $n_{^7\mathrm{Li}}$, at the temperature T is,

$$\begin{aligned} n_{^7\mathrm{Li}} &\sim 10^{-10} \cdot n_B \\ &= 10^{-10} \cdot \eta \cdot n_\gamma \\ &\simeq 1.9 \times 10^{-33} \cdot \left[\frac{T}{10\mathrm{keV}}\right] \cdot [\mathrm{fm}]^{-3} \\ &\simeq 5.7 \times 10^{-8} \cdot \left[\frac{T}{10\mathrm{keV}}\right] \cdot [\mathrm{barn}]^{-1}\ [\mathrm{sec}]^{-1}, \end{aligned} \tag{4.10}$$

where the baryon to photon ratio $\eta = 6.1 \times 10^{-10}$ and the number density of photon $n_\gamma = \frac{2\zeta(3)}{\pi^2}T^3$.

Further the processes (4.3) and (4.3) are cancel their effect each other. Part of the ^{7} created by the process (4.3) interact with $\tilde{\tau}^+$ and return to ^{7}Be. Therefore the net effect of these processes is suppressed. We thus conclude that the effect of the hadronic-current interaction with free staus is insufficient to solve the ^{7}Li problem.

4.2 Formation of stau–nucleus bound states

The interaction between a stau and a nucleus proceeds more efficiently when they form a bound state [29] due to two reasons.

1. The overlap of the wavefunctions of the two becomes large since the stau and nucleus are at a distance of the radius of the nucleus a_{nucl},

$$a_{\mathrm{nucl}} = 1.2 \times A^{\frac{1}{3}} \simeq 2.30\mathrm{fm}, \tag{4.11}$$

and packed in the small space. We note that the radius is not the Bohr radius of the bound state

$a_{\rm Bohr}$,

$$a_{\rm Bohr} = \frac{m_e}{Z m_{red}} a_0 \simeq 1.06 {\rm fm}. \tag{4.12}$$

Here the m_e is the electron mass, a_0 is the Bohr radius of hydrogen and m_{red} is the reduced mass of the bound state, defined by

$$m_{red} \equiv \frac{m_N m_{\tilde{\tau}}}{m_N + m_{\tilde{\tau}}} \simeq m_N, \tag{4.13}$$

where m_N is the mass of the nucleus. This is because the Bohr radius is shorter than the nuclear radius of ^{7}Be/^{7}Li, and therefore the stau is submerged in the nucleus and lose the Coulomb energy.

2. No cancellation process, like process (4.2), occur. Since only negatively-charged particles can form the bound state with nuclei, positively-charged staus can not form the bound state and induce cancellation processes.

The cross section of the formation of the bound state with the direct transition from the free state into the 1S bound state, σ_c, is given by Ref. [76, 19],

$$\begin{aligned} \sigma_c v &= \frac{2^9 \pi^2 \alpha Z_N^2}{3} \cdot \frac{E_{\rm bin}}{m_N^3 v} \cdot \left(\frac{E_{\rm bin}}{E_{\rm bin} + \frac{1}{2} m_N v^2} \right)^2 \cdot \frac{\exp\left[-4 \sqrt{\frac{2E_{\rm bin}}{m_N v^2}} \tan^{-1} \left(\sqrt{\frac{m_N v^2}{2E_{\rm bin}}} \right) \right]}{1 - \exp\left[-2\pi \sqrt{\frac{2E_{\rm bin}}{m_N v^2}} \right]} \\ &\simeq \frac{2^9 \pi^2 \alpha Z_N^2}{3 e^4} \cdot \frac{E_{\rm bin}}{m_N^3 v}. \end{aligned} \tag{4.14}$$

Here Z_N is the electric charge of the nucleus. $E_{\rm bin}$ is the binding energy of the bound state, and v is the relative velocity of the stau and the nucleus.

The thermal-averaged cross section is written as

$$\begin{aligned} \langle \sigma_c v \rangle &= \frac{1}{n_1 n_2} \left(\frac{g}{8\pi^3} \right)^2 \int d^3p_1 d^3p_2 e^{-\frac{(E_1+E_2)}{T}} \sigma_c v \\ &= \frac{1}{n_G n_r} \left(\frac{g}{8\pi^3} \right)^2 \int d^3p_G e^{-\frac{m_G}{T}} e^{-\frac{p_G^2}{2m_G T}} \int d^3p_r \sigma_c v e^{-\frac{p_r^2}{2m_{red} T}} \\ &= \frac{2^9 \pi \alpha Z_N^2 \sqrt{2\pi}}{3e^4} \frac{E_{\rm bin}}{m_N^2 \sqrt{m_N T}}, \end{aligned} \tag{4.15}$$

where $m_G = m_1 + m_2$ with

$$\begin{aligned} n_G &= \frac{g}{(2\pi)^3} \int d^3p_G e^{-\frac{m_G}{T}} e^{-\frac{p_G^2}{2m_G T}}, \\ n_r &= \frac{g}{(2\pi)^3} \int d^3p_r e^{-\frac{p_r^2}{2m_{red} T}}. \end{aligned}$$

Here we have assumed that only one stau is captured by a nucleus. Since the photon emission from a stau is suppressed, the cross section for the further capture of an additional stau by the bound state would be much smaller. Therefore, we ignore the multiple capture of staus by a nucleus.

The number density of the bound state is calculated by employing the Boltzmann equation,

$$\frac{d}{dt} n_{BS} + 3H n_{BS} = \langle \sigma_c v \rangle n_{\tilde{\tau}} n_N,$$

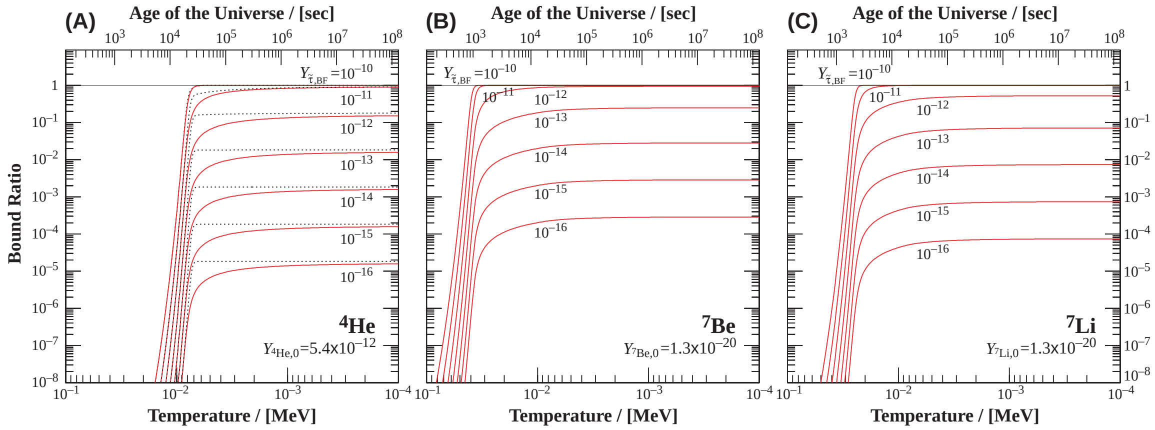

Figure 4.3: Evolutions of the bound ratio of the nuclei ^{4}He, ^{7}Be, and ^{7}Li. We vary the abundance of the stau at the time of the formation of the bound state from 10^{-10} to 10^{-16} in each figure. In Fig. 4.3(a), we also plotted by dotted lines corresponding curves predicted using the Saha equation for reference.

where n_{BS} shows the number density of the bound state, and H is the Hubble constant. We show in Fig. 4.3 the evolutions of the bound ratios of ^{4}He, ^{7}Li, and ^{7}Be, where we define the bound ratio by the number density of a nucleus that forms a bound state with a stau, divided by the total number density of that nucleus. Here $Y_{\tilde{\tau},\mathrm{BF}}$ is the yield value of staus at the time of *the formation of the bound state* with nuclei t_{BF}. $Y_{\tilde{\tau},\mathrm{BF}}$ is given by the the yield value of the staus at the *freeze-out* time $Y_{\tilde{\tau},\mathrm{FO}} \equiv n_{\tilde{\tau}}/s\,|_{\mathrm{Freeze\ Out}}$, and the lifetime of stau $\tau_{\tilde{\tau}}$, where $n_{\tilde{\tau}}$ and s are the densities of the number of staus and the entropy, respectively;

$$Y_{\tilde{\tau},\mathrm{BF}} = Y_{\tilde{\tau},\mathrm{FO}}\, \mathrm{e}^{-t_{\mathrm{BF}}/\tau_{\tilde{\tau}}}. \tag{4.16}$$

The difference between $Y_{\tilde{\tau},\mathrm{FO}}$ and $Y_{\tilde{\tau},\mathrm{BF}}$ will be significant when we consider in the short stau lifetime region. We will see it in chapter 5

4.3 Internal conversion of nuclei in the stau-nucleus bound state

The stau-nucleus bound state decays through the following processes

$$\tilde{\tau} + {}^7\mathrm{Be} \to (\tilde{\tau}\,{}^7\mathrm{Be}) \to \tilde{\chi}^0 + \nu_\tau + {}^7\mathrm{Li}, \tag{4.17}$$
$$\tilde{\tau} + {}^7\mathrm{Li} \to (\tilde{\tau}\,{}^7\mathrm{Li}) \to \tilde{\chi}^0 + \nu_\tau + {}^7\mathrm{He}, \tag{4.18}$$
$${}^7\mathrm{He} \to {}^6\mathrm{He} + \mathrm{n}, \tag{4.19}$$
$${}^6\mathrm{He} + \text{background particles} \to {}^3\mathrm{He}, {}^4\mathrm{He}, \text{etc.}, \tag{4.20}$$

where the parentheses denote the bound states. We note that we introduce not only reaction (4.17), but also reaction (4.18). The ^{6}He nucleus can also decay into ^{6}Li via β-decay with the lifetime 817 msec. We do not take this process into account since this process is much slower than the scattering process (4.20).

The lifetime of the internal conversion τ_{IC} is obtained from Eq. (4.6) and the overlap of the wave functions of the staus and the nucleus $|\psi|^2$, as

$$\tau_{\mathrm{IC}} = \frac{1}{|\psi|^2 \cdot (\sigma v)}. \tag{4.21}$$

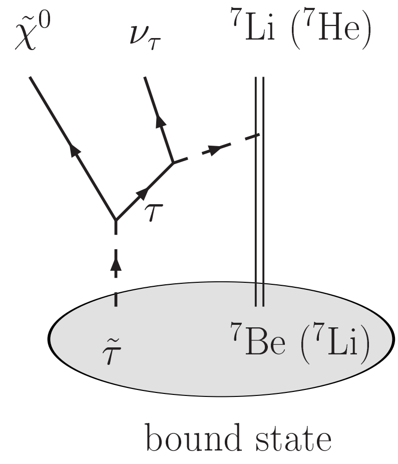

Figure 4.4: The Feynman diagrams of internal conversion of ^{7}Be (^{7}Li).

We estimate the overlap of the wave functions in Eq. (4.21) by assuming that the bound state is in the S-state of a hydrogen-like atom, and obtain

$$|\psi|^2 = \frac{1}{\pi a_{\rm nucl}^3}, \tag{4.22}$$

where $a_{\rm nucl}$ is the radius of the nucleus (see Eq. (4.11)).

Our new effects have been treated as if ^{7}Li or ^{7}Be in its bound state would have an effectively new lifetime which is caused by the virtual exchange of the hadronic current with a stau. Thus this new process is not the two-bodies scattering. So, there is no corresponding astrophysical S-factor in these processes.

The evaluated lifetimes of the reactions (4.17) and (4.18) under these approximations are presented in Fig. 4.5 as functions of δm. There we take $m_{\tilde{\chi}^0} = 300\,\mathrm{GeV}$, $\theta_\tau = \pi/3$, and $\gamma_\tau = 0$ for both reactions. We find that the lifetime of the internal conversion process is in the order of 10^{-3} sec. The lifetime of stau-^{7}Li bound state diverges around $\delta m = m_{^7\mathrm{Li}} - m_{^7\mathrm{Be}} = 11.7\,\mathrm{MeV}$, below which the internal conversion is kinematically forbidden.

4.4 Stau-catalyzed fusion

Another process to destroy the ^{7}Li/^{7}Be is nuclear fusion catalyzed by staus. A nucleus has a Coulomb barrier which normally prevents the nuclear fusion, while the barrier is weakened when a stau is captured to a state bound to the nucleus. The nuclear fusion is thus promoted by forming a stau-nucleus bound state. The stau serves as a catalyst and is left out as the fusion proceeds through.

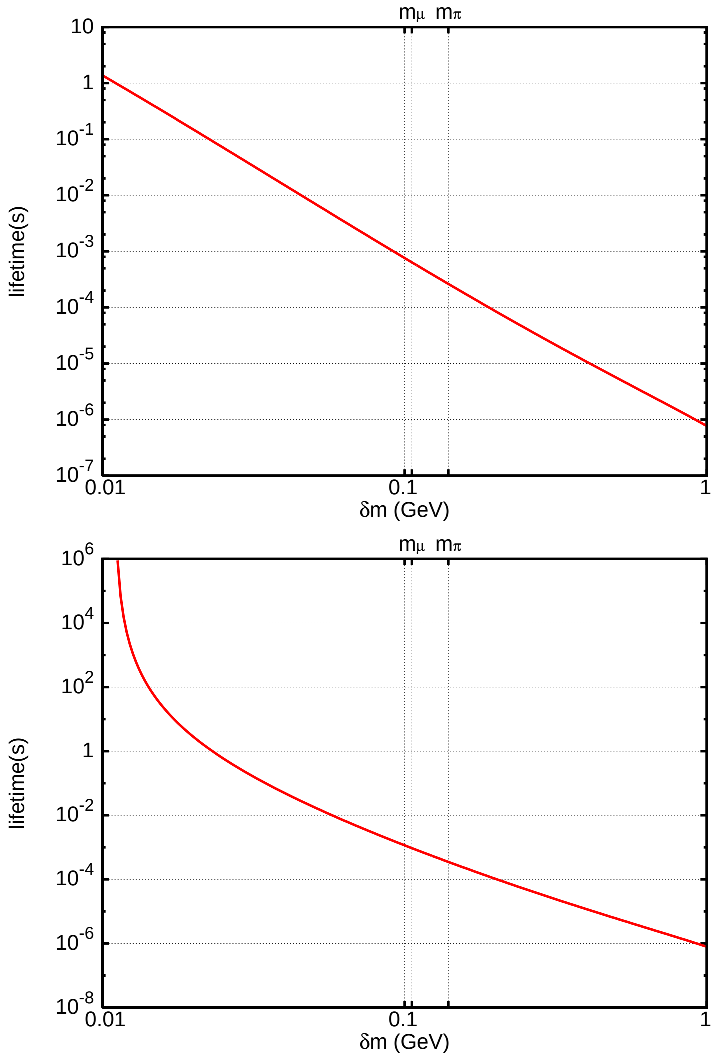

Figure 4.5: The lifetimes of internal conversion processes as the function of δm. Top panel: $(\tilde{\tau}^7\mathrm{Be}) \to \tilde{\chi}^0 + \nu_\tau + {}^7\mathrm{Li}$, bottom panel: $(\tilde{\tau}^7\mathrm{Li}) \to \tilde{\chi}^0 + \nu_\tau + {}^7\mathrm{He}$. We take $m_{\tilde{\chi}^0} = 300$ GeV, $\theta_\tau = \pi/3$ and $\gamma_\tau = 0$ in both figures.

The new ^{7}Li/^{7}Be decay channels are induced by the stau-catalyzed fusion process:

$$^7\mathrm{Be} + \tilde{\tau} \to (^7\mathrm{Be}\,\tilde{\tau}) + \gamma, \tag{4.23}$$
$$^7\mathrm{Li} + \tilde{\tau} \to (^7\mathrm{Li}\,\tilde{\tau}) + \gamma, \tag{4.24}$$
$$(^7\mathrm{Be}\,\tilde{\tau}) + \mathrm{p} \to (^8\mathrm{B}\,\tilde{\tau}) + \gamma, \tag{4.25}$$
$$(^7\mathrm{Be}\,\tilde{\tau}) + \mathrm{n} \to (^7\mathrm{Li}\,\tilde{\tau}) + \mathrm{p}, \tag{4.26}$$
$$\begin{aligned}(^7\mathrm{Li}\,\tilde{\tau}) + \mathrm{p} &\to \tilde{\tau} + 2\,^4\mathrm{He} \quad \text{or} \\ &\to \tilde{\tau} + 2\,\mathrm{D} + {}^4\mathrm{He}.\end{aligned} \tag{4.27}$$

The lifetime of the stau-catalyzed fusion is estimated to be longer than 1 sec [23]. Thus this process is less effective to reduce ^{7}Li and ^{7}Be than the internal conversion process. We follow Ref. [28] to calculate the stau-catalyzed fusion rate.

The stau-catalyzed fusion process is effective to produce ^{6}Li [18, 27, 77], $(\tilde{\tau}\,^4\mathrm{He}) + \mathrm{D} \to {}^6\mathrm{Li} + \tilde{\tau}$. This process becomes significant in the small δm region since the formation time of $(\tilde{\tau}\,^4\mathrm{He})$ is ten times later than that of $(\tilde{\tau}\,^7\mathrm{Li})$ and $(\tilde{\tau}\,^7\mathrm{Be})$, and a stau with large δm can not survive until the time. We will see this again in chapter 5.

Chapter 5

Numerical results

In this chapter we search a parameter region in which the ^{7}Li problem is solved, where we use numerical calculations. We will find that the parameter region actually appears and the solution gives strict constraint on supersymmetric parameters. We investigate the importance of the precise formation rate of the bound state by comparing the results due to the Saha equation and the Boltzmann equation.

5.1 Numerical calculation and interpretation of the result

In this section, we study the effectiveness of new decay channels on ^{7}Li reduction by numerical calculation. To do this, we choose the yield value of staus at freeze out time $Y_{\tilde{\tau},\mathrm{FO}}$ and the mass difference δm as free parameters. These values are sensitive to the abundance of ^{7}Be and ^{7}Li. The number of ^{7}Li interacted with the stau is determined by the number density of the stau and thus the yield value of staus at freeze out time. The hadronic decay rate of stau is mainly determined by the mass difference. The decay rate is also determined by the stau mixing angle $\theta_{\tilde{\tau}}$, CP violating phase γ_τ, and neutralino mass. As we showed in chapter 3, however, the effects by these parameters are much less than mass difference.

In Fig. 5.1 we show parameter region of δm and $Y_{\tilde{\tau}}$ allowed by the observational light-element abundances, where we take $\eta = 6.1 \times 10^{-10}$, $m_{\tilde{\chi}^0} = 300$ GeV, $\theta_\tau = \pi/3$ and $\gamma_\tau = 0$. The white region is the parameter space, which is consistent with all the observational abundance including that of ^{7}Li/H. The region enclosed by dashed lines is excluded by the observational abundance of ^{6}Li/^{7}Li [48], and the one enclosed by solid lines are allowed by those of ^{7}Li/H [47]. The thick dotted line is given by the upper bound of the yield value of dark matter

$$Y_{\mathrm{DM}} = 4.02 \times 10^{-12} \Big(\frac{\Omega_{\mathrm{DM}} h^2}{0.110}\Big)\Big(\frac{m_{\mathrm{DM}}}{10^2\,\mathrm{GeV}}\Big)^{-1}, \tag{5.1}$$

taking $\Omega_{\mathrm{DM}} h^2 = 0.1099 + 0.0124$ (upper bound of 95% confidence level) [79] and $m_{\mathrm{DM}} = m_{\tilde{\chi}^0}$. This line gives the upper bound of $Y_{\tilde{\tau},\mathrm{FO}}$, since the supersymmetric particles after their freeze-out consist of not only staus but neutralinos as well in our scenario.

The allowed region shown in Fig. 5.1 lies at $\delta m \simeq (100-120)\,\mathrm{MeV}$, which is tiny compared with $m_{\tilde{\chi}^0} = 300\,\mathrm{GeV}$. These values of parameters allow the coannihilation between neutralinos and staus, and thus can account also for the abundance of the dark matter. We therefore find that the values of $m_{\tilde{\chi}^0} = 300\,\mathrm{GeV}$ and $\delta m \simeq 100\,\mathrm{MeV}$ can simultaneously explain the abundance of dark matter and of ^{7}Li.

We compare the Figs. 5.1(a) and 5.1(b) to find that the allowed region is shifted downward in Fig. 5.1(b). Of the two processes included in Fig. 5.1(b), the resonant formation process makes the bound ratio larger, the value of $Y_{\tilde{\tau}}$ smaller, and push the allowed region downward in the figure. On the other hand, the photo dissociation process makes the bound ratio smaller through the destruction of the

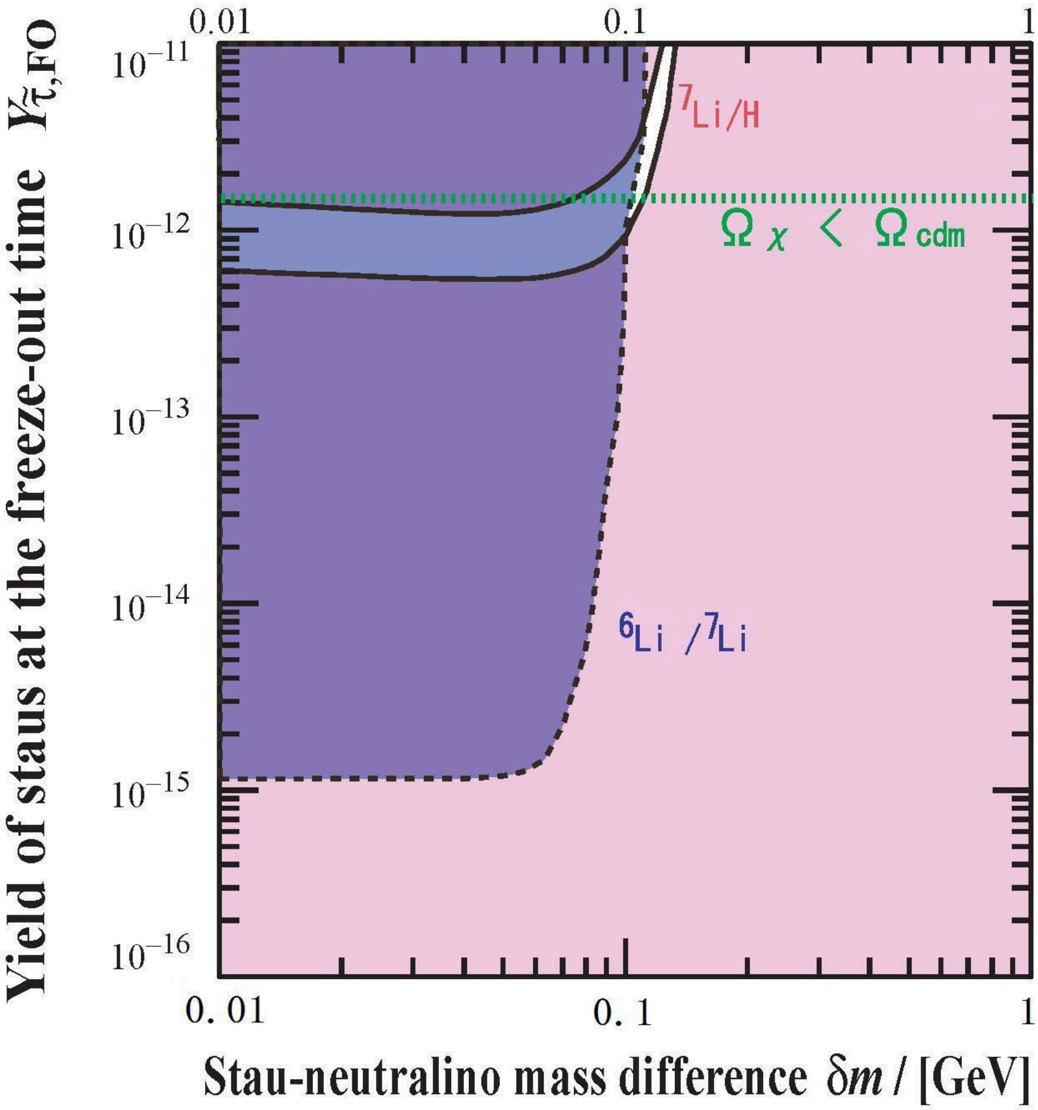

Figure 5.1: Allowed region in δm-$Y_{\tilde{\tau},\mathrm{FO}}$ plane. The white region is the parameter space, which is consistent with all the observational abundance including that of ^{7}Li/H. The region enclosed by dashed lines is excluded by the observational abundance of ^{6}Li/^{7}Li [48], and the one enclosed by solid lines are allowed by those of ^{7}Li/H [47]. The thick dotted line is given by the upper bound of the yield value of dark matter. This line gives the upper bound of $Y_{\tilde{\tau},\mathrm{FO}}$.

bound state, makes the value of $Y_{\tilde{\tau}}$ larger, and push the allowed region upward. We thus find that the resonant formation of the bound state is relevant while the photo dissociation is inconsequential.

The qualitative feature of the allowed region is explained from the following physical consideration. First, we note that $Y_{\tilde{\tau},\mathrm{FO}} \gtrsim (10^{-13}-10^{-12})$ is required so that a sufficient number of bound state $(\tilde{\tau}\,{}^7\mathrm{Be})$ is formed to destruct ^{7}Be by the internal conversion into ^{7}Li. The daughter ^{7}Li is broken either by an energetic proton or by the internal conversion $(\tilde{\tau}\,{}^7\mathrm{Li}) \to \tilde{\chi}^0 + \nu_\tau + {}^7\mathrm{He}$, and consequently ^{7}Li/H is reduced. Bearing this physical situation in mind, we consider parameter regions in detail.

1. $\delta m \gtrsim 120\,\mathrm{MeV}$.
   Since the staus decay before they form a bound state with ^{7}Be, the value of $Y_{\tilde{\tau},\mathrm{BF}}$ is much lower than 10^{-13} and hence the abundance of neither ^{7}Be nor ^{7}Li is reduced. Therefore this parameter region is excluded.

2. $100\,\mathrm{MeV} \lesssim \delta m \lesssim 120\,\mathrm{MeV}$.
   The staus are just decaying at the formation time of the bound state. The necessary condition of $Y_{\tilde{\tau},\mathrm{BF}} \sim 10^{-13}$ can still be retained even in a case where the value of $Y_{\tilde{\tau},\mathrm{FO}}$ is sufficiently large. The allowed region in this area of δm thus bends upward. In this region, a daughter ^{7}Li from the internal conversion of $(\tilde{\tau}\,{}^7\mathrm{Be})$ is broken mainly by an energetic proton.

3. $Y_{\tilde{\tau},\mathrm{FO}} \lesssim 10^{-13}$.
   In this case $Y_{\tilde{\tau},\mathrm{BF}}$ is necessarily less than 10^{-13}, and the bound ratio of ^{7}Li and ^{7}Be are much less than $O(1)$ as seen in Fig. 4.3. Therefore, the final abundance of ^{7}Li is not reduced sufficiently. This parameter region is thus excluded.

4. $Y_{\tilde{\tau},\mathrm{FO}} > 10^{-12}$ and $\delta m < 100\,\mathrm{MeV}$.
   In this region $Y_{\tilde{\tau},\mathrm{BF}} = Y_{\tilde{\tau},\mathrm{FO}} > 10^{-12}$ and hence the bound ratio of ^{7}Be is 1 (see Fig. 4.3). It means that ^{7}Be and consequently ^{7}Li are destructed too much. Hence, the upper-left region is excluded.

5. $\delta m \lesssim 100\,\mathrm{MeV}$ and $Y_{\tilde{\tau},\mathrm{FO}} \gtrsim 10^{-15}$.
   In this region, the stau acquires the long lifetime enough to form a bound state $(\tilde{\tau}\,{}^4\mathrm{He})$. Then the catalyzed fusion process $(\tilde{\tau}\,{}^4\mathrm{He}) + \mathrm{D} \to {}^6\mathrm{Li} + \tilde{\tau}$ leads to the overproduction of ^{6}Li and to the disagreement to the observational limit. Therefore, this parameter region is excluded, which is consistent with calculations by Ref. [28, 80].

Excluding all the parameter regions described above, we obtain a small allowed region of $m_{\tilde{\chi}^0} \simeq m_{\tilde{\tau}} \simeq 300\,\mathrm{GeV}$ and $\delta m = (100-120)\,\mathrm{MeV}$ as presented in Fig. 5.1, and these values are at the same time consistent to the coannihilation scenario of the dark matter.

5.2 Need for accurate evaluation of the formation rate

The numerical result strongly depends on the formation rate of the bound state. To see the dependence we consider in the limit of small expansion rate of the universe, and use the Saha equation;

$$n_{\mathrm{BS}} = \left(\frac{m_{\mathrm{N}} T}{2\pi}\right)^{-3/2} e^{E_{\mathrm{B}}/T} (n_{\mathrm{N}} - n_{\mathrm{BS}})(n_{\tilde{\tau}^-} - n_{\mathrm{BS}}), \tag{5.2}$$

instead of the Boltzmann equation. Here, n_{BS}, $n_{\tilde{\tau}}$, and n_{N} denote number densities of the bound state, the stau, and the nucleus, respectively; m_{N}, E_{B}, and T denote the nucleus mass, binding energy of the bound state, and the temperature of universe, respectively. The Saha equation coincide with the Boltzmann equation in the limit of small expansion rate of the universe. The expansion rate of the universe is not negligible in our case and therefore the formation rate becomes larger than of the Boltzmann equation.

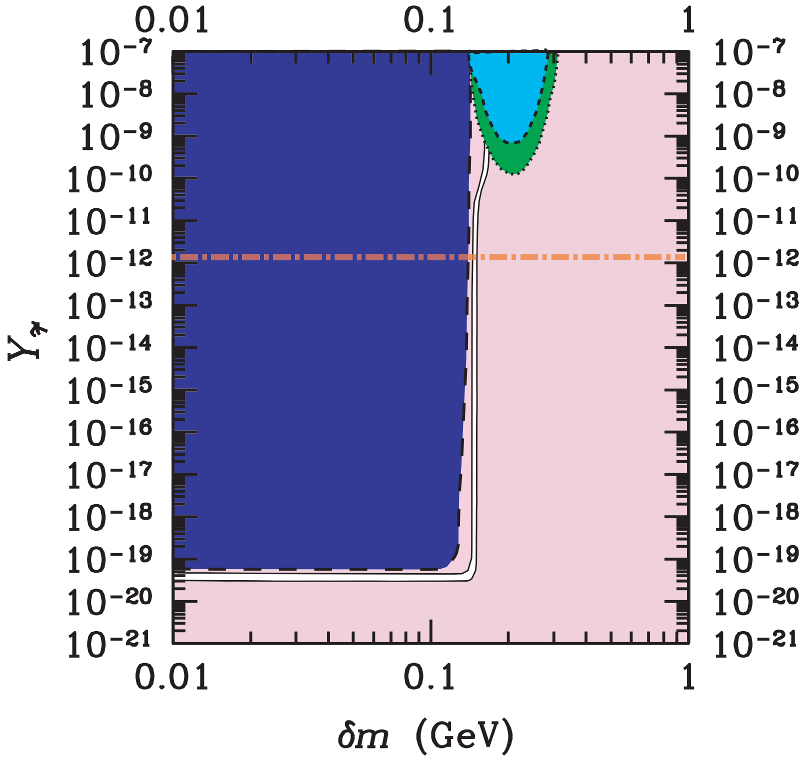

Figure 5.2: The constraints from the light-element abundance shown in the δm–$Y_{\tilde{\tau}}$ plane. The white region is the parameter space which is consistent with all the observational abundance including ^{7}Li/H=$(1.23^{+0.32}_{-0.25}) \times 10^{-10}$ [3]. The regions enclosed by dotted (green), dashed (light blue), and dash-dotted (purple) lines are excluded by the observations on ^{4}He, D and ^{6}Li, respectively. The thick-dotted line represents a yield value of stau whose daughter particle, neutralino, accounts for all the dark matter component. Here we took $\eta = 6.1 \times 10^{-10}$, $m_{\tilde{\chi}^0} = 300$ GeV, $\theta_\tau = \pi/3$ and $\gamma_\tau = 0$.

Thus it is suitable for the understanding of the dependence to compare the results of the Boltzmann equation with the Saha equation.

In Fig. 5.2 we show the parameter region of δm and $Y_{\tilde{\tau}}$ allowed by the observational light-element abundances, where we take $\eta = 6.1 \times 10^{-10}$, $m_{\tilde{\chi}^0} = 300$ GeV, $\theta_\tau = \pi/3$ and $\gamma_\tau = 0$. The white region is the parameter space which is consistent with all the observational abundance including ^{7}Li to hydrogen ratio (^{7}Li/H). The regions enclosed by dotted (green), dashed (light blue), and dash-dotted (purple) lines are excluded by the observations on the mass fraction of ^{4}He ($Y_{\rm p}$), deuterium to hydrogen ratio (D/H) and ^{6}Li to ^{7}Li ratio (^{6}Li/^{7}Li), respectively. The upper central region is excluded by the observational constrains on D/H and ^{4}He due to charged pions emitted from decaying staus [81, 82, 83, 84, 85].

From Fig. 5.2 we find that larger formation rate leads enough number of the bound state from smaller number density of staus, and consequently downward shift of the allowed region in $\delta m < 100$MeV. Thus accurate evaluation of the formation rate of the bound state is important.

Chapter 6

Summary

We summarize this thesis here. At first we studied the big-bang nucleosynthesis which predicts primordial abundances of light elements only with one parameter, baryon-to-photon ratio η, where we investigated both of the theoretical and the experimental view points. The theoretical study of the big-bang nucleosynthesis is developed over fifty years, and its uncertainty becomes small. Hence at the observed value of η determined by recent WMAP experiment [1] the theoretical values for ^{4}He, D and ^{3}He are coincident with observed values at least in 2 σ confidence interval (see Fig. 2.2). Nevertheless the predicted and observed values are different for ^{7}Li. This discrepancy is called the ^{7}Li problem.

We discussed the possible solution to the ^{7}Li problem. We consider the possibility to explain the ^{7}Li problem by uncertainties of the observation. Indeed the uncertainties of the stellar process may not be ignored due to the lack of our astrophysical knowledge, e.g. the convection in stars. However the uncertainties are not enough to explain the ^{7}Li problem. We thus searched and the solution, and found that it is given by processes of beyond the standard model, especially supersymmetric model.

Next we have studied an MSSM scenario in which the LSP and NLSP are a bino-like neutralino and a stau, respectively. Since the mass difference is, in many cases, assumed to be degenerate, from the requirement of coannihilation, we paid special attention to the very small δm case. We calculated the partial lifetimes for the decay modes shown in Fig. 3.1.

We have investigated the stau lifetime dependence on δm, θ_τ, γ_τ, and $m_{\tilde{\chi}}$. The lifetime strongly depends on δm and θ_τ, while it is almost independent of γ_τ and $m_{\tilde{\chi}}$. The dependence on δm of stau lifetime changes as each threshold is crossed. When δm is larger than m_τ, the lifetime increases in proportion to $(\delta m)^{-2}$ as δm decreases. In the range $m_\tau > \delta m > m_\pi$ the lifetime obeys the scaling $\sim (\delta m)^{-6}$. Below m_π, it grows with $(\delta m)^{-8}$. The δm dependence of the stau lifetime can be largely understood by counting the mass dimension of phase space and the squared amplitude in the massless limit of Standard Model particles. While the massless limit is a good approximation in regions far from the thresholds, the δm dependence near the thresholds are given by Eq. (3.18). The lifetime also strongly depends on θ_τ, as shown in Fig. 3.5. $\tilde{\tau}_R$ contributes to 3- and 4-body decay processes by picking up the m_τ term in the intermediate τ propagator, while $\tilde{\tau}_L$ picks up the p_τ term. Since $p_\tau \sim \delta m \ll m_\tau$, the contribution for $\tilde{\tau}_R$ is much larger and hence there is a strong dependence on θ_τ.

We have also discussed lepton flavor violation due to slepton mixing. If there is even a tiny component of a scalar electron or a scalar muon in the NLSP "stau", the decay signal of the NLSP will be completely different from the pure stau case. The NLSP slepton undergoes 2-body decay into the accompanying electron or muon. Since it is a 2-body process, it occurs very quickly, $\sim (10^{-20})N_1^{-2}$ sec where N_1 represents the portion of the scalar electron or scalar muon, as shown in Eq. (3.19). As this mixing causes charged/neutral lepton flavor violation, it is very important to compare the NLSP slepton decay with other processes such as $\tau \to e(\mu)\gamma$. To fully clarify the nature of the NLSP, we need to interpret all the LFV processes together.

We obtained a strict constraint on the mass of the neutralinos and staus by improving an analysis of a solution to the overproduction problem of ^{7}Li and ^{7}Be through the internal conversion in stau-nucleus bound states, $(\tilde{\tau}\,^7\mathrm{Be}) \to \tilde{\chi}^0 + \nu_\tau + {}^7\mathrm{Li}$ and $(\tilde{\tau}\,^7\mathrm{Li}) \to \tilde{\chi}^0 + \nu_\tau + {}^7\mathrm{He}$, given in Ref. [86]. We used the Boltzmann equation to estimate number density of the stau-nucleus bound states. By varying the yield value of the stau at its freeze-out time, we found that most of ^{7}Li and ^{7}Be nuclei form a bound state with a stau for $Y_{\tilde{\tau},\mathrm{BF}} \gtrsim (10^{-12} - 10^{-13})$. Taking the values of $m_{\tilde{\chi}^0} = 300\,\mathrm{GeV}$, $\theta_\tau = \pi/3$, $\gamma_\tau = 0$, and $\eta = (6.225 \pm 0.170) \times 10^{-10}$ [79], we obtained a parameter region consistent with the observed abundance of ^{7}Li within $Y_{\tilde{\tau},\mathrm{FO}} = (7-10) \times 10^{-13}$ and $\delta m = (100-120)\,\mathrm{MeV}$. The region of $\delta m \leq 100\,\mathrm{MeV}$ is excluded due to the overproduction of ^{6}Li by the catalyzed fusion. Furthermore, the parameter region obtained in this thesis lies in the coannihilation region, which can explain the relic abundance of dark matter. Therefore, the stau with $m_{\tilde{\tau}} \sim 300\,\mathrm{GeV}$ and $\delta m \sim 100\,\mathrm{MeV}$ can simultaneously solve the problems on the relic abundance of the light elements and the dark matter.

We also compared the numerical results due to the Boltzmann equation and the Saha equation and found that the precise determination of the formation rate of the bound state is important to derive the allowed parameter region.

As shown in Fig. 3.3, the stau with $m_{\tilde{\tau}} = 300\,\mathrm{GeV}$ and $\delta m = 100\,\mathrm{MeV}$ has the lifetime of $O(100-1000)$ sec. It is very possible that Large Hadron Collider (LHC) and the International Linear Collider (ILC) will find some staus with a very long lifetime [87, 73, 74]. In our scenario we should observe very low energy π, μ, or e, as contrasted to the gravitino LSP scenario [70, 71, 72] in which energetic τ is apparently produced. Therefore a clean experiment is required. The ILC would be most suitable for investigating the nature of the NLSP slepton. These collider studies may gives experimental evidence of our scenario. The author expect for the progress of the experiments.

Acknowledgments

I would like to express my gratitude to my supervisor, Professor Joe Sato, whose expertise, understanding, and patience. I learned physics, expertise, approach to research, and everything needed to earn a degree.

I appreciate Professor Yoshiaki Tanii for his significant lectures and seminars, and Professor Naotaka Yoshinaga and Professor Takeshi Suzuki for valuable comments on my thesis and research. I also appreciate my collaborators, Masafumi Koike, Kazunori Kohri, Takashi Shimomura and Masato Yamanaka, for collaboration with my research and meaningful discussions. I sincerely appreciate Professor Masayasu Kamimura and Professor Koichi Yazaki for valuable discussions and comments on my research. All the members of my laboratory support my student life in various ways. I am grateful to them. Finally I would like to thank to all of the friends and family.

I could not finish my doctoral program without any help from these people. I would like to thank everyone.

Appendix A

Decay rates of the stau

In this appendix, we show the exact and approximate stau decay rates. We use the exact decay rate in formulating the figures. We make the following approximations: we keep only the leading order term of $(\delta m/m_{\tilde{\chi}})$ and we replace the denominator of the τ propagator by m_τ^2 in the 3- and 4-body cases. We calculate the decay rates of the three processes shown in Fig. 3.1 with the Lagrangian of Eq. (3.5).

1. **2-body decay**
   The decay rate of the 2-body decay process (see Fig. 3.1(a)) is given by

$$\begin{aligned}\Gamma_{\text{2-body}} = & \frac{1}{16\pi m_{\tilde{\tau}}^3}(m_{\tilde{\tau}}^4 + m_{\tilde{\chi}^0}^4 + m_\tau^4 - 2m_{\tilde{\tau}}^2 m_{\tilde{\chi}^0}^2 - 2m_{\tilde{\tau}}^2 m_\tau^2 - 2m_{\tilde{\chi}^0}^2 m_\tau^2)^{\frac{1}{2}} \\ & \times\Big\{(g_L^2 + |g_R|^2)(m_{\tilde{\tau}}^2 - m_{\tilde{\chi}^0}^2 - m_\tau^2) - 4Re[g_L g_R] m_\tau m_{\tilde{\chi}^0}\Big\} \ . \end{aligned} \tag{A.1}$$

   For the analysis discussed in Sec. 3.2, we approximate the decay rate as

$$\Gamma_{\text{2-body}} = \frac{1}{4\pi m_{\tilde{\chi}^0}}\sqrt{(\delta m)^2 - m_\tau^2}\left((g_L^2 + |g_R|^2)\delta m - 2Re[g_L g_R] m_\tau\right) \ . \tag{A.2}$$

2. **3-body decay**
   The decay rate of the 3-body decay process (see Fig. 3.1(b)) is calculated as

$$\begin{aligned}\Gamma_{\text{3-body}} = & \frac{G^2 f_\pi^2 \cos^2\theta_c \left((\delta m)^2 - m_\pi^2\right)}{64\pi^3 m_{\tilde{\tau}}^3} \\ & \times \int_0^1 dx \sqrt{\left((\delta m)^2 - q_f^2\right)\left((\delta m + 2m_{\tilde{\chi}^0})^2 - q_f^2\right)} \ \frac{1}{(q_f^2 - m_\tau^2)^2 + (m_\tau \Gamma_\tau)^2} \\ & \times \frac{(q_f^2 - m_\pi^2)^2}{2q_f^2}\left[\frac{1}{4}(g_L^2 q_f^2 + |g_R^2| m_\tau^2)((\delta m)^2 + 2m_{\tilde{\chi}^0}\delta m - q_f^2) - Re[g_L g_R] m_{\tilde{\chi}^0} m_\tau q_f^2\right] \ . \end{aligned} \tag{A.3}$$

   Here q_f^2 is given as

$$q_f^2 = (\delta m)^2 - \left((\delta m)^2 - m_f^2\right) x \ , \tag{A.4}$$

   where the index $f(= \pi, e, \mu)$ denotes a massive particle, except the neutralino, in the final states; $f = \pi$ in the 3-body case. Γ_τ is the tau decay width and $(m_\tau\Gamma_\tau)^2$ is added to the denominator of the tau propagator for the region $\delta m \geq m_\tau$.

The approximate decay rate is

$$\Gamma_{\text{3-body}} = \frac{G^2 f_\pi^2 \cos^2\theta_c}{105(2\pi)^3 m_{\tilde{\chi}^0} m_\tau^4} \delta m \left((\delta m)^2 - m_\pi^2\right)^{7/2} \left[g_L^2 - 2Re[g_L g_R]\frac{m_\tau}{\delta m} + \frac{7}{4}|g_R|^2 \frac{m_\tau^2}{(\delta m)^2}\right] \tag{A.5}$$

3. **4-body decay**
In the 4-body decay processes (see Fig. 3.1(c)), the decay rate is given by

$$\begin{aligned}
\Gamma_{\text{4-body}} =& \frac{G^2\left((\delta m)^2 - m_l^2\right)}{24(2\pi)^5 m_\tau^3} \\
&\times \int_0^1 dx \sqrt{\left((\delta m)^2 - q_f^2\right)\left((\delta m + 2m_{\tilde{\chi}^0})^2 - q_f^2\right)} \frac{1}{(q_f^2 - m_\tau^2)^2 + (m_\tau \Gamma_\tau)^2} \frac{1}{q_f^4} \\
&\times \left[\left\{\frac{1}{4}(g_L^2 q_f^2 + |g_R^2| m_\tau^2)((\delta m)^2 + 2m_{\tilde{\chi}^0}\delta m - q_f^2) - Re[g_L g_R] m_{\tilde{\chi}^0} m_\tau q_f^2\right\}\right. \\
&\times \left.\left\{12 m_l^4 q_f^4 \log\left[\frac{q_f^2}{m_l^2}\right] + (q_f^4 - m_l^4)(q_f^4 - 8m_l^2 q_f^2 + m_l^4)\right\}\right],
\end{aligned} \tag{A.6}$$

where $l = e, \mu$ and q_l^2 is given by Eq. (A.4).

We can approximate the decay rate as

$$\begin{aligned}
\Gamma_{\text{4-body}} =& \frac{G^2}{945(2\pi)^5 m_{\tilde{\chi}^0} m_\tau^4}\left((\delta m)^2 - m_l^2\right)^{5/2} \\
&\times \Big[2g_L^2 (\delta m)^3 \left(2(\delta m)^2 - 19m_l^2\right) - 4Re[g_L g_R] m_\tau (\delta m)^2 \left(2(\delta m)^2 - 19 m_l^2\right) \\
&\quad + 3|g_R|^2 m_\tau^2 \delta m \left(2(\delta m)^2 - 23 m_l^2\right)\Big]\,.
\end{aligned} \tag{A.7}$$

Appendix B

Evaluation of hadronic transition by ft-value

In this appendix we evaluate the amplitude of hadronic transition by ft-value. Here we investigate a transition ${}^7\mathrm{Be} \to {}^7\mathrm{Li}$ and its amplitude $\langle {}^7\mathrm{Li}|J_\mu|{}^7\mathrm{Be}\rangle$.

First we derive the ft-value by considering a β-decay. The interaction hamiltonian describing a β-decay is,

$$H_\beta = \frac{G}{\sqrt{2}}(\bar{\Psi}_p \gamma_\mu \tau_+ \Psi_n)(\bar{\psi}_e \gamma^\mu \psi_{\nu_e}), \tag{B.1}$$

where C_V is a coupling constant, and ψ_e and ψ_{ν_e} are the wavefunctions of electron and neutrino, respectively. Ψ_p and Ψ_n are the wavefunction of nucleon written in the isospin formula. We can rewrite them by four component spinor of proton ψ_p and neutron ψ_n as,

$$\Psi_p = \begin{pmatrix} \psi_p \\ 0 \end{pmatrix}, \ \Psi_n = \begin{pmatrix} 0 \\ \psi_n \end{pmatrix}. \tag{B.2}$$

τ_+ is a isospin increasing operator, which increase z component of isospin one

$$\tau_+ = \frac{1}{2}(\tau_x + i\tau_y), \tag{B.3}$$

where τ_x, τ_y and τ_z are the Pauli matrices. An operator which decrease z component of isospin one is,

$$\tau_- = \frac{1}{2}(\tau_x - i\tau_y). \tag{B.4}$$

This operator changes a proton into a neutron, and thus induce orbital electron capture.

We investigate the probability of a β-decay $P(E_e)$. A probability of emitting a electron with energy E_e in the unit time is,

$$P(E_e)dE_e = 2\pi |H_{fi}|^2 \frac{dn}{dE_l}. \tag{B.5}$$

Here E_l denotes the total energy of leptons (electron and neutrino) in final state, and dn/dE_0 is the density of such states. The transition matrix element H_{fi} is

$$H_{fi} = \frac{G}{\sqrt{2}} \int d\mathbf{x} (\Psi_p^\dagger \tau_+ \Psi_n)(\psi_e^\dagger \psi_{\nu_e}). \tag{B.6}$$

Here we neglect the components which corresponds to $\mu = 1, 2, 3$ and consider only $\mu = 0$ since we ignore the recoil of the protons and neutrons.

The Eq. (B.6) is made of three parts; (1) transition of baryon, (2) transition of lepton and (3) density of states. First we investigate individually each part, and later we assemble the results and find the probability and ft-value.

1. transition of baryon
   In this study we consider a nucleon decay in a nucleus. Therefore we modify the baryon part of the transition matrix element (B.6) to superposition of each nucleon decay,

   $$(\Psi_p^\dagger \tau_+ \Psi_n) \rightarrow \left(\Psi_f^\dagger \sum_{k=1}^{A} \tau_+^{(k)} \Psi_i \right), \tag{B.7}$$

   since each nucleon can induce β-decay.

2. transition of lepton
   The lepton part of the transition matrix element is discussed here. We consider the normalization of the wavefunctions of electron and neutrino as,

   $$\int \psi^\dagger \psi d\mathbf{x} = 1. \tag{B.8}$$

   Therefore the wavefunctions is written as

   $$\psi = \left(\frac{1}{V} \right)^{1/2} \exp\left(\frac{i\mathbf{p} \cdot \mathbf{x}}{\hbar} \right). \tag{B.9}$$

   Here we omit a factor representing spin for simplify. By taking long-wavelength approximation and supposing that wavefunction is constant in the nuclei *, we can evaluate the wavefunction by the value in the center of the nuclei,

   $$\psi_e = \psi_{\nu_e} = \left(\frac{1}{V} \right)^{1/2}. \tag{B.10}$$

   Assembling the Eqs. (B.7) and (B.10) the transition matrix element becomes

   $$H_{fi} = \frac{G}{\sqrt{2}V} \int 1 \tag{B.11}$$

   $$\int 1 \equiv \int \Psi_f^\dagger \sum_{k=1}^{A} \tau_+^{(k)} \Psi_i d\mathbf{x_1} d\mathbf{x_2} \cdots d\mathbf{x_A}. \tag{B.12}$$

   Here $\int 1$ represents the baryonic part of the transition matrix element.

3. density of states
   We consider the density of states corresponding to that one particle with certain spin direction exist

*Indeed the wavelengths of leptons are $\mathcal{O}(10)$–$\mathcal{O}(100)$ fm and 10–100 times larger than the radius of nuclei, since the typical energy of the lepton made by a β-decay is $\mathcal{O}(1)$–$\mathcal{O}(10)$ MeV.

in volume V and its momentum is between p and $p + dp$. The density is written as,

$$dn_1 = \frac{4\pi p^2 dpV}{h^3} = \frac{p^2 dpV}{2\pi^2}. \tag{B.13}$$

The density of state with total energy of the lepton between E_l and $E_l + dE_l$ is

$$\frac{dn}{dE_l} = \frac{dn_e dn_\nu}{dE_l} = \frac{V^2}{4\pi^4}\frac{p_e^2 dp_e p_\nu^2 dp_\nu}{dE_l}, \tag{B.14}$$

where p_ν is the energy of the neutrino. We rewrite this equation by electron energy E_e and E_l substitute for p_e and p_ν

$$\frac{dn}{dE_l} = \frac{V^2}{4\pi^4}\sqrt{E_e^2 - m_e^2}E_e(E_l - E_e)^2 dE_e. \tag{B.15}$$

Here m_e is the mass of the electron.

By substituting the Eqs (B.11) and (B.15) into Eq. (B.6), the probability becomes

$$P(E_e)dE_e = \frac{G^2}{4\pi^3}\left|\int 1\right|^2 \sqrt{E_e^2 - m_e^2}E_e(E_l - E_e)^2 dE_e. \tag{B.16}$$

We include a correction of the Coulomb interaction between the electron and the nucleus in the equation of the probability. This correction modify the Eq. (B.16) as,

$$P(E_e)dE_e = \frac{G^2}{4\pi^3}\left|\int 1\right|^2 F(\pm Z, E)\sqrt{E_e^2 - m_e^2}E_e(E_l - E_e)^2 dE_e. \tag{B.17}$$

$$F(\pm Z, E) = 2(1+\gamma)(2pR)^{2\gamma-2}\exp(\pm\pi\nu)\frac{|\Gamma(\gamma \pm i\nu)|^2}{[\Gamma(2\gamma+1)]^2} \tag{B.18}$$

$$\gamma = (1-\alpha^2 Z^2)^{1/2}, \quad \nu = \frac{\alpha Z E}{p}. \tag{B.19}$$

Here Γ is the Gamma functionAR is the radius of the nucleusA α is fine structure constant and Z shows the electric charge in the unit of electron charge e. The upper (lower) sign of the double sign in Eq. (B.19) corresponds to the correction to e^- (e^+). Here $F(\pm Z, E)$ is known as the Fermi function.

We define a value f called the integrated Fermi function. We rewrite Eq. (B.16) by dimensionless parameters; $\eta \equiv E/m_e$, $\eta_e \equiv E_e/m_e$, $\eta_l \equiv E_l/m_e$,

$$P(E_e)dE_e = \frac{m_e^5 G^2}{4\pi^3}\left|\int 1\right|^2 F(\pm Z, \eta)\sqrt{\eta_e^2 - 1}\eta_e(\eta_l - \eta_e)^2 d\eta_e. \tag{B.20}$$

f is defined as the integration of the right hand side of Eq. (B.20);

$$f \equiv f(\pm Z, E_0) = \int_1^{\eta_0} F(\pm Z, E_e)\sqrt{E_e^2 - m_e^2}E_e(E_0 - E_e)^2 dE_e. \tag{B.21}$$

Due to Eq. (B.21), we can obtain the ft-value. The probability of the β-decay is,

$$P = \frac{m_e^5 G^2}{4\pi^3}\left|\int 1\right|^2 f. \tag{B.22}$$

The probability can be replaced by the half-life period $t_{1/2}$,

$$P = \frac{1}{\tau} = \frac{\log 2}{t_{1/2}}. \tag{B.23}$$

The ft-value is defined as a product of the integrated Fermi function (Eq. (B.21)) and the half-life period appearing in Eq. (B.23),

$$ft \equiv f \cdot t_{1/2} = \frac{4\pi^3 \log 2}{m_e^5 G^2} \frac{1}{\left|\int 1\right|^2} \tag{B.24}$$

The dimension of the ft-value is of time. The ft-value is sometimes represented as logarithmic value $\log \frac{ft}{1 \text{ sec}}$. For example, a ft-value of a transition ${}^14O(0^+) \rightarrow {}^{14}N^*(0^+)$ is represented 3142 sec or 3.5.

In this appendix we simply consider only the interaction induced by Eq. (B.1) since it is enough to understand the relation between the amplitude of hadronic transition and ft-value. However there are other interactions describing β-decay, for example,

$$\begin{aligned} &C_A(\bar{\Psi}_p i\gamma_\mu\gamma_5\tau_+\Psi_n)(\bar{\psi}_e i\gamma^\mu\gamma_5\psi_{\nu_e}) + h.c. \\ =&C_A\left\{(\psi_p^\dagger \boldsymbol{\sigma}\tau_+\psi_n)(\psi_e^\dagger\boldsymbol{\sigma}\psi_{\nu_e}) - (\psi_p^\dagger\gamma_5\tau_+\psi_n)(\psi_e^\dagger\gamma_5\psi_{\nu_e})\right\} + h.c.\ . \end{aligned} \tag{B.25}$$

(B.26)

Here σ is defined as,

$$\boldsymbol{\sigma} = \begin{pmatrix} \sigma & 0 \\ 0 & \sigma \end{pmatrix}. \tag{B.27}$$

The hamiltonian

$$\int \sigma \equiv \Psi_f^\dagger \sum_{k=1}^{A} \boldsymbol{\sigma}\tau_+^{(k)}\Psi_i d\mathbf{x_1}d\mathbf{x_2}\cdots d\mathbf{x_A} \tag{B.28}$$

contribute to the Gamow-Teller transition, and ft-value should be modified as,

$$ft = \frac{4\pi^3 \log 2}{m_e^5} \frac{1}{G^2\left|\int 1\right|^2 + C_A^2\left|\int \sigma\right|^2}. \tag{B.29}$$

Contributions from other interactions are much smaller than above two interactions, $\int 1$ and $\int \sigma$. The transitions led by the other interactions are called forbidden transition, while led by $\int 1$ and $\int \sigma$ are called allowed transition.

Finally we should discuss the normalization of the baryonic part of the transition matrix element. In this appendix we have taken nonrelativistic normalization,

$$\langle \mathbf{P}|\mathbf{P'}\rangle = (2\pi)^3\delta^{(3)}(\mathbf{P} - \mathbf{P'}). \tag{B.30}$$

We, however, use relativistic normalization,

$$\langle \mathbf{P}|\mathbf{P'}\rangle = 2E_{\mathbf{P}}(2\pi)^3\delta^{(3)}(\mathbf{P} - \mathbf{P'}), \tag{B.31}$$

in the main body of this thesis. For consistency with the main body we rewrite the baryonic part of the transition matrix element Eq. B.12,

$$\int 1 = \frac{\langle {}^7\mathrm{Li}|J_\mu|{}^7\mathrm{Be}\rangle}{\sqrt{2E_{Be}}\sqrt{2E_{Li}}}. \tag{B.32}$$

We thus find the relation between the amplitude and ft-value in the relativistic normalization,

$$\left|\langle {}^7\mathrm{Li}|J_\mu|{}^7\mathrm{Be}\rangle\right|^2 = \frac{16\pi^3 E_{Be}E_{Li}\log 2}{m_e^5 G^2}\frac{1}{ft}. \tag{B.33}$$

Appendix C

Estimation method of the strength of β-decay

In this chapter we investigate the estimation way of the strength of β-decay to evaluate experimentally undetermined ft-value. The strength of the β-decay is determined by "changes of nuclear total spin and parity" and "overlap of initial and final wavefunctions".

C.1 Changes of nuclear total spin and parity

As mentioned in chapter B β-decay is described by some interactions. Each interaction contribute different changes of nuclear total spin and parity. Therefore β-decays with same changes have typical ft-value [88] (see Table C.1).

C.2 Overlap of initial and final wavefunctions; iso-multiplet

Although the changes for allowed transition are same with for superallowed transition, the typical ft-value for allowed transition is 100 times larger than for superallowed transition. This difference is due to the overlap of initial and final wavefunctions. In this section we investigate iso-multiplet formed by nuclei since iso-multiplet is important to understand the internal structure of nucleus and thus overlap of the wavefunctions. We note that in spite of the isospin symmetry is actually broken, we can treat it as a *good* symmetry in nuclei.

forbidden level	change of nuclear total spin	change of parity	$\log ft$
superallowed	0 (for Fermi), ±1 (for GT)	No	~ 3
allowed	0 (for Fermi), ±1 (for GT)	No	~ 5
first-forbidden	0, ±1, ±2	Yes	~ 7
second-forbidden	±2, ±3	No	~ 11
third-forbidden	±3, ±4	Yes	~ 15
nth-forbidden	$\pm n$, $\pm(n+1)$	$(-1)^n$ (1=Yes, -1=No)	$\sim 4n+3$

Table C.1: The relation between forbidden level, change of nuclear total spin and parity and typical ft-value.

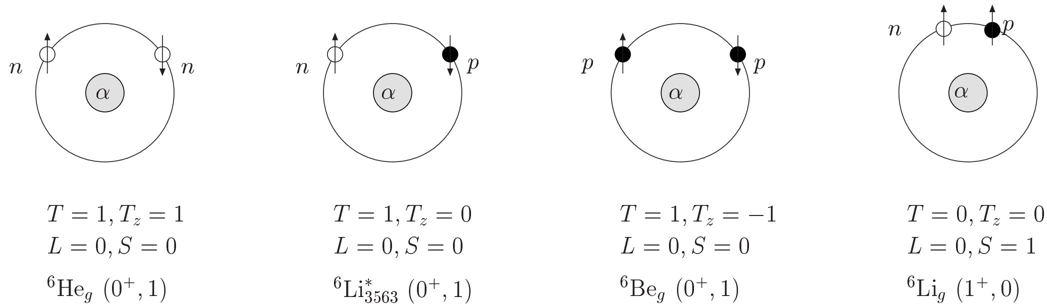

Figure C.1: The internal structure of $^6\mathrm{He}_g(0^+,1)$, $^6\mathrm{Be}_g(0^+,1)$, $^6\mathrm{Li}^*_{3563}(0^+,1)$ and $^6\mathrm{Li}_g(1^+,0)$. First three nuclei are in iso-triplet, and last nucleus is in iso-singlet.

C.2.1 2-nucleons system

We start with simplest case of iso-multiplet, 2-nucleons system. The isospin T and its z-component T_z of neutron n and proton p are,

$$n: \quad T = 1/2 \quad T_z = +1/2, \tag{C.1}$$

$$p: \quad T = 1/2 \quad T_z = -1/2. \tag{C.2}$$

The difference between neutron and proton is only the sign of T_z under the isospin symmetry. Therefore two nucleons form iso-triplet with $T = 1$ and iso-singlet with $T = 0$,

$$\text{iso-triplet} \cdots \begin{cases} (nn)_{T=1,T_z=+1,L=0,S=0} \\ (pp)_{T=1,T_z=-1,L=0,S=0} \\ (np)_{T=1,T_z=0,L=0,S=0} \end{cases}, \tag{C.3}$$

$$\text{iso-singlet} \cdots (np)_{T=0,T_z=0,L=0,S=1}, \tag{C.4}$$

where L and S indicate total angular momentum and total spin. In the 2-nucleons system with $T = 1$ the nucleons are weakly attracted and do not form a bound state, while with $T = 0$ the nucleons are strongly attracted and form a bound state as deuteron.

C.2.2 nuclei with $A = 6$

Next we consider the nuclei with mass number $A = 6$, ^{6}He, ^{6}Be and ^{6}Li. The structure of these nuclei is well explained by a picture; ^{4}He core and orbiting two nucleons (see Fig. C.1). In Fig. C.1 structure of the ground states of ^{6}He, ^{6}Be and ^{6}Li and of the excited state with exciting energy 3563 keV of ^{6}Li is shown. Here the ground states of ^{6}He, ^{6}Be and ^{6}Li are denoted as $^6\mathrm{He}_g$, $^6\mathrm{Be}_g$ and $^6\mathrm{Li}_g$, respectively, and the excited state of ^{6}Li is denoted as $^6\mathrm{Li}^*_{3563}$, where the subscript g indicates ground state, the superscript indicates excited state and subscript number indicates the exciting energy. The numbers and sign in parenthesis indicate total angular momentum, parity and isospin of the nucleus, e.g. $(0^+,1)$ shows that total angular momentum is zero, parity is plus and isospin is one. The arrows shows the direction of nuclear spin, in this regard, however there are other combinations of directions of arrows. Foe example the combination with downward n spin and upward p spin for $^6\mathrm{Li}^*_{3563}$ is also allowed.

Nuclei in different iso-multiplet have different internal structure. In $^6\mathrm{He}_g$ and $^6\mathrm{Be}_g$ and $^6\mathrm{Li}^*_{3563}$ two nucleons are in iso-triplet. The internal structures of the three nuclei in iso-triplet are similar since the difference is only the direction of iso-spin. The similarity is found from energy level of these nuclei (see

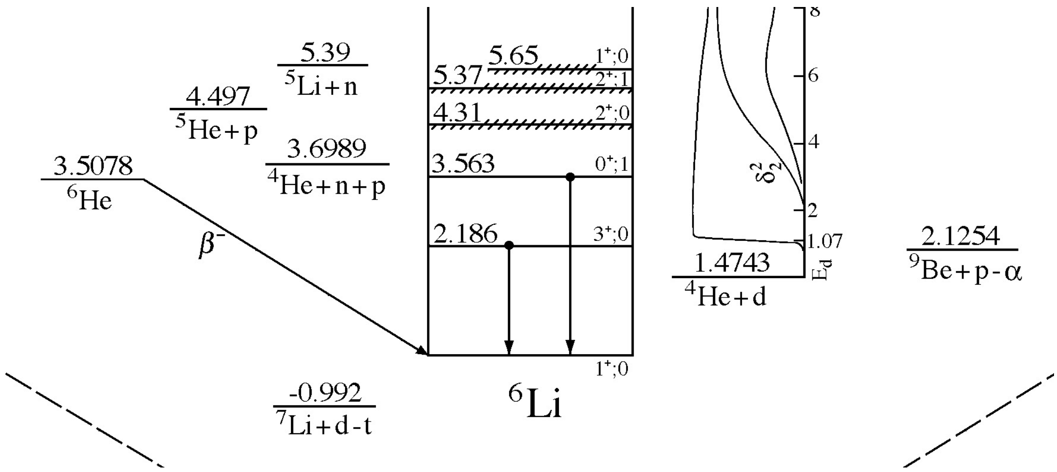

Figure C.2: The energy level of nuclei with $A = 6$. ${}^6\mathrm{Li}^*_{3563}$ and ${}^6\mathrm{He}_g(0^+,1)$ belong to same iso-triplet.

Fig. C.2). In Fig. C.2 ${}^6\mathrm{Li}^*_{3563}$ and ${}^6\mathrm{He}_g$ are in similar energy level (${}^6\mathrm{Be}_g$ is out of this figure). In the iso-triplet nuclei two nucleons are separated from each other. On the other hand in iso-singlet nucleus, ${}^6\mathrm{Li}_g$, two nucleons are close. Therefore the internal structures of nuclei in iso-triplet and in iso-singlet are different. Thus transition with the change of iso-multiplet are suppressed since the overlap of the wavefunctions is small.

C.2.3 nuclei with $A = 7$

Finally we consider the nuclei with $A = 7$, and estimate the ft-value of the transitions discussed in chapter 4 The structure of these nuclei with $A = 7$ is ${}^4\mathrm{He}$ core and orbiting three nucleons. These nuclei are well understood by the cluster model, in which we consider the nuclei as two-body system of ${}^4\mathrm{He}$ and a nucleus with three nucleons. The three nucleon system forms iso-quadruplet, ${}^7\mathrm{He}_g(\frac{3}{2}^-,\frac{3}{2})$, ${}^7\mathrm{Li}^*_{11240}(\frac{3}{2}^-,\frac{3}{2})$, ${}^7\mathrm{Be}^*_{11010}(\frac{3}{2}^-,\frac{3}{2})$ and ${}^7\mathrm{B}_g(\frac{3}{2}^-,\frac{3}{2}$, and iso-doublet, ${}^7\mathrm{Li}_g(\frac{3}{2}^-,\frac{1}{2})$ and ${}^7\mathrm{Be}_g(\frac{3}{2}^-,\frac{1}{2}$. These isomultiplet is found from energy level of these nuclei (see Fig. C.2). We consider the iso-quadruplet and the iso-doublet nuclei by a shell of the nuclei with three nucleons (see Figs. C.4 and C.5).

The transition from ${}^7\mathrm{Be}_g(\frac{3}{2}^-,\frac{1}{2}$ to ${}^7\mathrm{Li}_g(\frac{3}{2}^-,\frac{1}{2})$ easily occurs since both of the nuclei belong to same iso-multiplet. Indeed the ft-value for the transition is 3.3.

C.3 Estimation of ft-value

We investigate investigate the estimation way of the strength of β-decay, in other words ft-value. Due to the above sections we can evaluate a transition as superallowed transition ($ft \sim 3$) if it satisfies the following two conditions;

1. change of total nuclear spin is 0 or ± 1.
2. both of the initial and final states belong to same iso-multiplet.

The second condition might not be useful. Then we can use substitute condition; both of the states are in similar energy levels, such as ${}^6\mathrm{He}_g(0^+,1)$ and ${}^6\mathrm{Li}^*_{3563}(0^+,1)$.

We found estimation way for superallowed transitions, however there is a exception to the way. It is transition from ${}^6\mathrm{He}_g(0^+,1)$ to ${}^6\mathrm{Li}_g(1^+,0)$. The ft-value of the transition is 2.9. Above discussions can not explain the smallness of the ft-value.

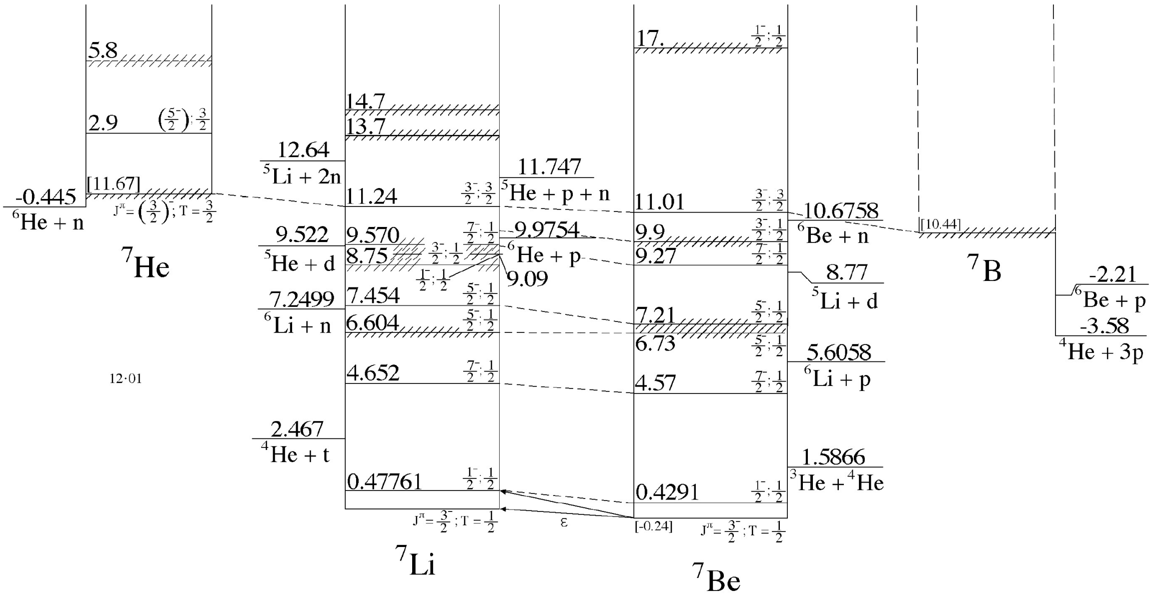

Figure C.3: The energy level of these nuclei with $A = 7$. $^7\mathrm{He}_g(\frac{3}{2}^-,\frac{3}{2})$, $^7\mathrm{Li}^*_{11240}(\frac{3}{2}^-,\frac{3}{2})$, $^7\mathrm{Be}^*_{11010}(\frac{3}{2}^-,\frac{3}{2})$ and $^7\mathrm{B}_g(\frac{3}{2}^-,\frac{3}{2}$ belong to iso-quadruplet, and $^7\mathrm{Li}_g(\frac{3}{2}^-,\frac{1}{2})$ and $^7\mathrm{Be}_g(\frac{3}{2}^-,\frac{1}{2})$ belong to iso-doublet.

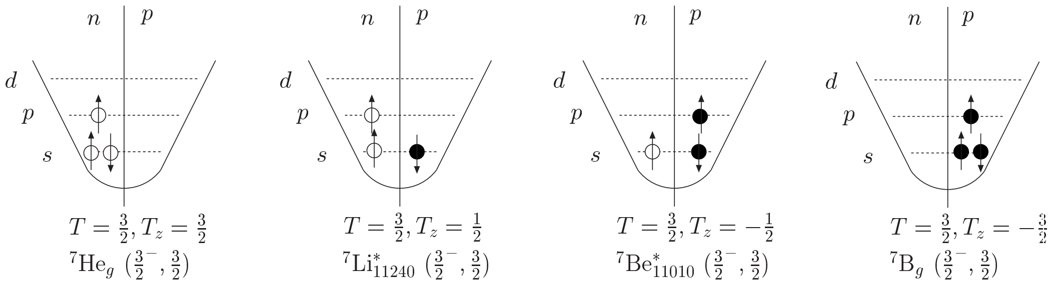

Figure C.4: The levels of three nucleons in the shell of $^7\mathrm{He}_g(\frac{3}{2}^-,\frac{3}{2})$, $^7\mathrm{Li}^*_{11240}(\frac{3}{2}^-,\frac{3}{2})$, $^7\mathrm{Be}^*_{11010}(\frac{3}{2}^-,\frac{3}{2})$ and $^7\mathrm{B}_g(\frac{3}{2}^-,\frac{3}{2})$. These nuclei belong to iso-quadruplet. Here, the white and black circle indicate n and p, respectively.

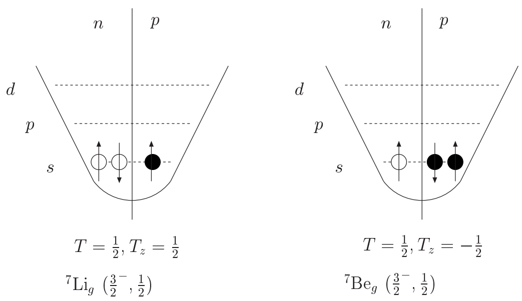

Figure C.5: The levels of three nucleons in the shell of $^7\mathrm{Li}_g(\frac{3}{2}^-,\frac{1}{2})$ and $^7\mathrm{Be}_g(\frac{3}{2}^-,\frac{1}{2})$. These nuclei belong to iso-doublet. Here, the white and black circle indicate n and p, respectively.

From the existence of the exception we can expect that ft-value of the transition between ${}^7\mathrm{He}_g(\frac{3}{2}^-,\frac{3}{2})$ and ${}^7\mathrm{Li}_g(\frac{3}{2}^-,\frac{1}{2})$ is also small. Thus for the transition between ${}^7\mathrm{He}_g(\frac{3}{2}^-,\frac{3}{2})$ and ${}^7\mathrm{Li}_g(\frac{3}{2}^-,\frac{1}{2})$ we use $ft = 3.3$ which is same with the transition between ${}^7\mathrm{Li}_g(\frac{3}{2}^-,\frac{1}{2})$ and ${}^7\mathrm{Be}_g(\frac{3}{2}^-,\frac{1}{2})$.

Bibliography

[1] D. N. Spergel et al. Wilkinson Microwave Anisotropy Probe (WMAP) three year results: Implications for cosmology. *Astrophys. J. Suppl.*, 170:377, 2007.

[2] Alain Coc, Elisabeth Vangioni-Flam, Pierre Descouvemont, Abderrahim Adahchour, and Carmen Angulo. Updated Big Bang Nucleosynthesis confronted to WMAP observations and to the Abundance of Light Elements. *Astrophys. J.*, 600:544–552, 2004.

[3] S. G. Ryan, T. C. Beers, Keith A. Olive, B. D. Fields, and J. E. Norris. Primordial Lithium and Big Bang Nucleosynthesis. *Astrophys. J. Lett*, 530:L57, 2000.

[4] Richard H. Cyburt, Brian D. Fields, and Keith A. Olive. Primordial Nucleosynthesis in Light of WMAP. *Phys. Lett.*, B567:227–234, 2003.

[5] P. Bonifacio et al. The lithium content of the globular cluster NGC 6397. *Astron. Astrophys.*, 390:91, 2002.

[6] Jorge Melendez and Ivan Ramirez. Reappraising the Spite Lithium Plateau: Extremely Thin and Marginally Consistent with WMAP. *Astrophys. J.*, 615:L33, 2004.

[7] Richard H. Cyburt, Brian D. Fields, and Keith A. Olive. Solar Neutrino Constraints on the BBN Production of Li. *Phys. Rev.*, D69:123519, 2004.

[8] C. Angulo et al. The 7Be(d,p)2alpha cross section at Big Bang energies and the primordial 7-Li abundance. *Astrophys. J.*, 630:L105–L108, 2005.

[9] Andreas J. Korn et al. A probable stellar solution to the cosmological lithium discrepancy. *Nature*, 442:657–659, 2006.

[10] Kazuhide Ichikawa and Masahiro Kawasaki. Big bang nucleosynthesis with a varying fine structure constant and non-standard expansion rate. *Phys. Rev.*, D69:123506, 2004.

[11] Kazuhide Ichikawa, Masahiro Kawasaki, and Fuminobu Takahashi. Solving the discrepancy among the light elements abundances and WMAP. *Phys. Lett.*, B597:1–10, 2004.

[12] Karsten Jedamzik. Did something decay, evaporate, or annihilate during big bang nucleosynthesis? *Phys. Rev.*, D70:063524, 2004.

[13] Karsten Jedamzik, Ki-Young Choi, Leszek Roszkowski, and Roberto Ruiz de Austri. Solving the cosmic lithium problems with gravitino dark matter in the CMSSM. *JCAP*, 0607:007, 2006.

[14] Kazunori Kohri, Takeo Moroi, and Akira Yotsuyanagi. Big-bang nucleosynthesis with unstable gravitino and upper bound on the reheating temperature. *Phys. Rev.*, D73:123511, 2006.

[15] Robert N. Cahn and Sheldon L. Glashow. Chemical Signatures for Superheavy Elementary Particles. *Science*, 213:607–611, 1981.

[16] A. De Rujula, S. L. Glashow, and U. Sarid. CHARGED DARK MATTER. *Nucl. Phys.*, B333:173, 1990.

[17] Savas Dimopoulos, David Eichler, Rahim Esmailzadeh, and Glenn D. Starkman. GETTING A CHARGE OUT OF DARK MATTER. *Phys. Rev.*, D41:2388, 1990.

[18] Maxim Pospelov. Particle physics catalysis of thermal big bang nucleosynthesis. *Phys. Rev. Lett.*, 98:231301, 2007.

[19] Kazunori Kohri and Fumihiro Takayama. Big Bang Nucleosynthesis with Long Lived Charged Massive Particles. *Phys. Rev.*, D76:063507, 2007.

[20] Manoj Kaplinghat and Arvind Rajaraman. Big bang nucleosynthesis with bound states of long-lived charged particles. *Phys. Rev.*, D74:103004, 2006.

[21] Richard H. Cyburt, John R. Ellis, Brian D. Fields, Keith A. Olive, and Vassilis C. Spanos. Bound-state effects on light-element abundances in gravitino dark matter scenarios. *JCAP*, 0611:014, 2006.

[22] Frank Daniel Steffen. Constraints on Gravitino Dark Matter Scenarios with Long- Lived Charged Sleptons. *AIP Conf. Proc.*, 903:595–598, 2007.

[23] K. Hamaguchi, T. Hatsuda, and T. T. Yanagida Yanagida. Stau-catalyzed nuclear fusion. 2006.

[24] Daniele Fargion and M. Khlopov. Tera-leptons shadows over sinister universe. 2005.

[25] Daniele Fargion, M. Khlopov, and Christoph A. Stephan. Cold dark matter by heavy double charged leptons? *Class. Quant. Grav.*, 23:7305–7354, 2006.

[26] K. M. Belotsky, M. Yu. Khlopov, and K. I. Shibaev. Composite Dark Matter and its Charged Constituents. *Grav. Cosmol.*, 12:93–99, 2006.

[27] K. Hamaguchi, T. Hatsuda, M. Kamimura, Y. Kino, and T. T. Yanagida. Stau-catalyzed Li-6 production in big-bang nucleosynthesis. *Phys. Lett.*, B650:268–274, 2007.

[28] Masahiro Kawasaki, Kazunori Kohri, and Takeo Moroi. Big-Bang Nucleosynthesis with Long-Lived Charged Slepton. *Phys. Lett.*, B649:436–439, 2007.

[29] Chris Bird, Kristen Koopmans, and Maxim Pospelov. Primordial Lithium Abundance in Catalyzed Big Bang Nucleosynthesis. *Phys. Rev.*, D78:083010, 2008.

[30] Toshifumi Jittoh, Joe Sato, Takashi Shimomura, and Masato Yamanaka. Long life stau. *Phys. Rev.*, D73:055009, 2006.

[31] David Tytler, John M. O'Meara, Nao Suzuki, and Dan Lubin. Review of Big Bang Nucleosynthesis and Primordial Abundances. *Phys. Scripta*, T85:12, 2000.

[32] C. Amsler et al. Review of particle physics. *Phys. Lett.*, B667:1, 2008.

[33] Brian D. Fields and Keith A. Olive. Big bang nucleosynthesis. *Nucl. Phys.*, A777:208–225, 2006.

[34] Jr. R. A. Alpher, J. W. Follin and R. C. Herman. Physical Conditions in the Initial Stages of the Expanding Universe. *Phys. Rev.*, 92:1347, 1953.

[35] P. J. E. Peebles. Primordial Helium Abundance and the Primordial Fireball. II. *Astrophys. J.*, 146:542, 1966.

[36] F. Hoyle R. V. Wagoner, W. A. Fowler. On the Synthesis of Elements at Very High Temperatures. *Astrophys. J.*, 148:3, 1967.

[37] R. V. Wagoner. Big-Bang Nucleosynthesis Revisited. *Astrophys. J.*, 179:343, 1973.

[38] Lawrence Kawano. Let's Go: Early Universe. Guide to Primordial Nucleosynthesis Programming. FERMILAB-PUB-88-034-A.

[39] Keith A. Olive and Evan D. Skillman. A Realistic Determination of the Error on the Primordial Helium Abundance: Steps Toward Non-Parametric Nebular Helium Abundances. *Astrophys. J.*, 617:29, 2004.

[40] Yuri I. Izotov, T. X. Thuan, and G. Stasinska. The primordial abundance of 4He: a self-consistent empirical analysis of systematic effects in a large sample of low-metallicity HII regions. *Astrophys. J.*, 662:15–38, 2007.

[41] Brian E. Wood et al. Two New Low Galactic D/H Measurements from FUSE. *Astrophys. J.*, 609:838–853, 2004.

[42] T. M. Bania, Robert T. Rood, and Dana S. Balser. The cosmological density of baryons from observations of $^3He^+$ in the Milky Way. *Nature*, 415:54–57, 2002.

[43] J. Geiss and G. Gloeckler. Isotopic Composition of H, HE and NE in the Protosolar Cloud. *Space Science Reviews*, 106:3–18, April 2003.

[44] F. Spite M. Spite. Lithium abundance at the formation of the Galaxy. *Nature*, 297:483–485, 1982.

[45] P. E. Nissen and W. J. Schuster. Chemical composition of halo and disk stars with overlapping metallicities. *Astron. Astrophys.*, 326:751–762, October 1997.

[46] Brian D. Fields and Keith A. Olive. The Evolution of Li6 in Standard Cosmic-Ray Nucleosynthesis. 1998.

[47] Piercarlo Bonifacio et al. First stars VII. Lithium in extremely metal poor dwarfs. *Astron. Astrophys.*, 462:851–864, 2007.

[48] Martin Asplund, David L. Lambert, Poul Erik Nissen, Francesca Primas, and Verne V. Smith. Lithium isotopic abundances in metal-poor halo stars. *Astrophys. J.*, 644:229–259, 2006.

[49] Tijana Prodanovic and Brian D. Fields. On Non-Primordial Deuterium Production by Accelerated Particles. *Astrophys. J.*, 597:48–56, 2003.

[50] H. Reeves, J. Audouze, W. A. Fowler, and D. N. Schramm. On the Origin of Light Elements. *Astrophys. J.*, 179:909–930, February 1973.

[51] R. I. Epstein. The origin of deuterium, September 1976.

[52] Olivier Richard, Georges Michaud, and Jacques Richer. Implications of WMAP observations on Li abundance and stellar evolution models. *Astrophys. J.*, 619:538–548, 2005.

[53] S. Kato. *A basic theory of astrophysics.* gotou syobou., 1989.

[54] S. N. Ahmed et al. Measurement of the total active B-8 solar neutrino flux at the Sudbury Neutrino Observatory with enhanced neutral current sensitivity. *Phys. Rev. Lett.*, 92:181301, 2004.

[55] D. N. Spergel et al. First Year Wilkinson Microwave Anisotropy Probe (WMAP) Observations: Determination of Cosmological Parameters. *Astrophys. J. Suppl.*, 148:175, 2003.

[56] C. L. Bennett et al. First Year Wilkinson Microwave Anisotropy Probe (WMAP) Observations: Preliminary Maps and Basic Results. *Astrophys. J. Suppl.*, 148:1, 2003.

[57] Gerard Jungman, Marc Kamionkowski, and Kim Griest. Supersymmetric dark matter. *Phys. Rept.*, 267:195–373, 1996.

[58] Lars Bergstrom. Non-baryonic dark matter: Observational evidence and detection methods. *Rept. Prog. Phys.*, 63:793, 2000.

[59] Carlos Munoz. Dark matter detection in the light of recent experimental results. *Int. J. Mod. Phys.*, A19:3093–3170, 2004.

[60] Gianfranco Bertone, Dan Hooper, and Joseph Silk. Particle dark matter: Evidence, candidates and constraints. *Phys. Rept.*, 405:279–390, 2005.

[61] H. Goldberg. Constraint on the photino mass from cosmology. *Phys. Rev. Lett.*, 50:1419, 1983.

[62] John R. Ellis, J. S. Hagelin, Dimitri V. Nanopoulos, Keith A. Olive, and M. Srednicki. Supersymmetric relics from the big bang. *Nucl. Phys.*, B238:453–476, 1984.

[63] John R. Ellis, Toby Falk, Keith A. Olive, and Mark Srednicki. Calculations of neutralino stau coannihilation channels and the cosmologically relevant region of MSSM parameter space. *Astropart. Phys.*, 13:181–213, 2000.

[64] Kim Griest and David Seckel. Three exceptions in the calculation of relic abundances. *Phys. Rev.*, D43:3191–3203, 1991.

[65] Benjamin W. Lee and Steven Weinberg. Cosmological lower bound on heavy-neutrino masses. *Phys. Rev. Lett.*, 39:165–168, 1977.

[66] Junji Hisano, Shigeki Matsumoto, and Mihoko M. Nojiri. Explosive dark matter annihilation. *Phys. Rev. Lett.*, 92:031303, 2004.

[67] Shigeki Matsumoto, Joe Sato, and Yoshio Sato. Enhancement of line gamma ray signature from Bino-like dark matter annihilation due to CP violation. 2005.

[68] Stefano Profumo, Kris Sigurdson, Piero Ullio, and Marc Kamionkowski. A running spectral index in supersymmetric dark-matter models with quasi-stable charged particles. *Phys. Rev.*, D71:023518, 2005.

[69] A. V. Gladyshev, D. I. Kazakov, and M. G. Paucar. Production of long-lived sleptons at LHC. *Mod. Phys. Lett.*, A20:3085–3094, 2005.

[70] Jonathan L. Feng, Shufang Su, and Fumihiro Takayama. Supergravity with a gravitino LSP. *Phys. Rev.*, D70:075019, 2004.

[71] Koichi Hamaguchi and Alejandro Ibarra. Probing lepton flavour violation in slepton NLSP scenarios. *JHEP*, 02:028, 2005.

[72] Xiao-Jun Bi, Jian-Xiong Wang, Chao Zhang, and Xin-min Zhang. Phenomenology of quintessino dark matter. *Phys. Rev.*, D70:123512, 2004.

[73] Koichi Hamaguchi, Yoshitaka Kuno, Tsuyoshi Nakaya, and Mihoko M. Nojiri. A study of late decaying charged particles at future colliders. *Phys. Rev.*, D70:115007, 2004.

[74] Jonathan L. Feng and Bryan T. Smith. Slepton trapping at the Large Hadron and International Linear Colliders. *Phys. Rev.*, D71:015004, 2005.

[75] W. B. Lin, D. H. Huang, X. Zhang, and Robert H. Brandenberger. Non-thermal production of WIMPs and the sub-galactic structure of the universe. *Phys. Rev. Lett.*, 86:954, 2001.

[76] E. E. Salpeter H. A. Bethe. *Quantun Mechanics of One-and Two- Electron Atoms*. Springer-Verlag, 1957.

[77] Masayasu Kamimura, Yasushi Kino, and Emiko Hiyama. Big-Bang Nucleosynthesis Reactions Catalyzed by a Long- Lived Negatively-Charged Leptonic Particle. 2008.

[78] Howard E. Haber and Gordon L. Kane. The Search for Supersymmetry: Probing Physics Beyond the Standard Model. *Phys. Rept.*, 117:75–263, 1985.

[79] J. Dunkley et al. Five-Year Wilkinson Microwave Anisotropy Probe (WMAP) Observations: Likelihoods and Parameters from the WMAP data. 2008.

[80] Masahiro Kawasaki, Kazunori Kohri, Takeo Moroi, and Akira Yotsuyanagi. Big-Bang Nucleosynthesis and Gravitino. 2008.

[81] M. H. Reno and D. Seckel. Primordial Nucleosynthesis: The Effects of Injecting Hadrons. *Phys. Rev.*, D37:3441, 1988.

[82] Kazunori Kohri. Primordial nucleosynthesis and hadronic decay of a massive particle with a relatively short lifetime. *Phys. Rev.*, D64:043515, 2001.

[83] Masahiro Kawasaki, Kazunori Kohri, and Takeo Moroi. Big-bang nucleosynthesis and hadronic decay of long-lived massive particles. *Phys. Rev.*, D71:083502, 2005.

[84] Masahiro Kawasaki, Kazunori Kohri, and Takeo Moroi. Hadronic decay of late-decaying particles and big-bang nucleosynthesis. *Phys. Lett.*, B625:7–12, 2005.

[85] Karsten Jedamzik. Big bang nucleosynthesis constraints on hadronically and electromagnetically decaying relic neutral particles. *Phys. Rev.*, D74:103509, 2006.

[86] Toshifumi Jittoh et al. Possible solution to the ^{7}Li problem by the long lived stau. *Phys. Rev.*, D76:125023, 2007.

[87] A. De Roeck et al. Supersymmetric benchmarks with non-universal scalar masses or gravitino dark matter. *Eur. Phys. J.*, C49:1041–1066, 2007.

[88] A. Fujii K. Yamada, M. Morita. *Beta-decay and Weak Interaction*. Baifukan., 1974.